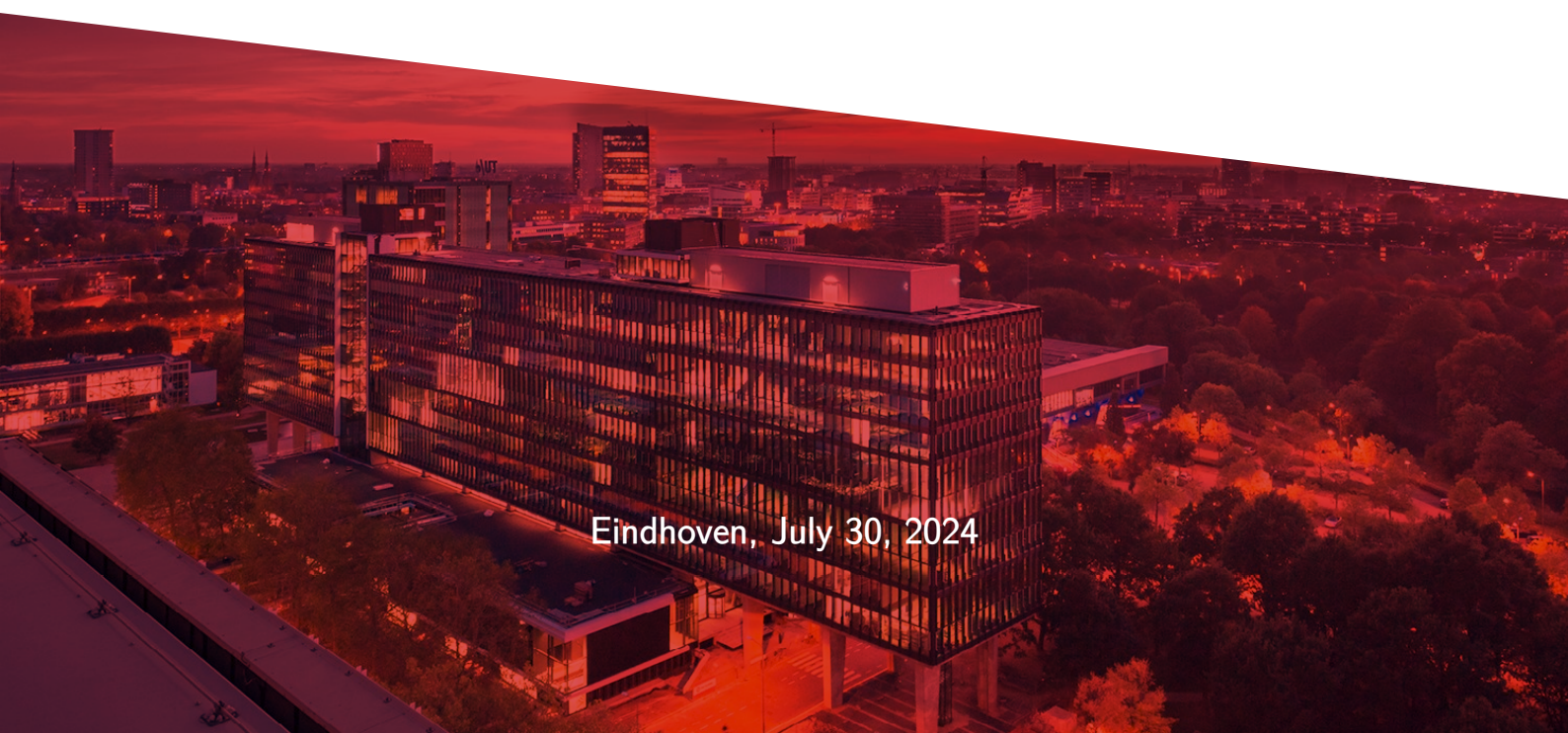


Group 10

Full Name	Student ID
Malik Weren	1788701
Ben Lentschig	1824805
Codrin Danculea	1886266
Daniel Tyukov	1819283
Ivan Stojic	1852876
Jasper Kadijk	1880969
Martin Genchev	1812033
Radu Cretu	1793918
Youri Lamers	1676865

A wide-angle aerial photograph of the TU/e campus in Eindhoven, Netherlands, during sunset. The sky is filled with warm orange and red hues. In the foreground, a large modern building with a glass facade is prominent, surrounded by green trees. The background shows a dense urban area with numerous other buildings and infrastructure.

Eindhoven, July 30, 2024

Contents

1	Introduction	3
1.1	Project Background	3
1.2	Project Statement	3
1.3	Challenge	3
1.4	Architecture	1
2	System design	2
2.1	General System	2
3	Energy source (Youri Lamers)	3
4	Load (Youri Lamers)	4
5	Power electronics	5
5.1	Introduction	5
5.2	DC/DC Converter (Malik Weren)	5
5.3	DC/AC Converter (Jasper Kadijk)	10
5.4	DC/AC Converter (Youri Lamers)	13
6	Magnetics (Radu Cretu & Codrin Danculea)	14
6.1	Coil Design (Cretu Radu)	14
6.2	Methods (Optimization Code) (Codrin Danculea)	16
6.3	Optimization Results (Codrin Danculea)	19
6.4	Coil Parameters (Cretu Radu)	20
6.5	Conclusion (Codrin Danculea)	21
7	PCB Design	22
7.1	DC/DC design choices (Daniel Tyukov)	23
7.2	DC/AC design choices (Martin Genchev)	27
8	Microcontroller (Ben Lentschig)	30
8.1	Feedback loop principle	30
8.2	Nucleo-32 F303k8 Board details	30
8.3	Timer and ADC configurations	31
8.4	Voltage measurements	31
8.5	Current measurements	31
8.6	DC/DC implementation	32
8.7	DC/AC implementation	32
8.8	Maximum power point transfer	33
8.9	Load detection	33
8.10	Results	34
9	Simulink model (Ivan Stojic & Youri Lamers)	35
9.1	Introduction - Ivan Stojic	35
9.2	Analysis of the Generator Design in the Converter System - Ivan Stojic	35
9.3	Analysis of the DC/DC Converter Design - Ivan Stojic	36
9.4	Analysis of the DC/AC Converter Design - Ivan Stojic	37
9.5	Analysis of Coil Configuration in the Converter System - Ivan Stojic	38
9.6	Analysis of the AC-DC Converter Design - Ivan Stojic	39
9.7	General Alternative Design Considerations - Youri Lamers	40
9.8	Power and efficiency calculations - Youri Lamers	40
9.9	Predictions and Testing results - Youri Lamers	42

10 Testing	44
10.1 DC/DC testing (Daniel Tyukov)	44
10.2 DC/AC testing (Jasper Kadijk)	44
10.3 Coils testing (Codrin Danculea)	44
10.4 Microcontroller testing (Ben Lentschig)	44
11 Conclusions and Recommendations	46
11.1 Conclusion	46
11.2 Recommendation	46
12 References	47
A f303k8 tolerances	48
B Specifications IRF640NPBF MOSFET	49
C IR2110PBF High side and low side driver circuit	49
D MATLAB script for DC/DC converter component selection	49
E Picture of final setup	50
F Appendix B: Magnetics	51
F.1 Optimization script	51

1 | Introduction

1.1 | Project Background

In the evolving landscape of office technology, the integration of wireless power systems represents a significant step forward in streamlining workspace environments. This project, undertaken by a collaborative team within the Wireless Energy Transfer Collaborative Learning Block, aims to develop a robust wireless charging system capable of powering desktop PCs. By eliminating the clutter of cables, this system not only enhances aesthetic appeal but also increases functionality in dynamic office settings, including adjustable desks.

1.2 | Project Statement

The primary objective of this project is to design and implement a wireless charging system that meets specific performance criteria:

- Deliver a minimum of 100W power output.
- Enable effective energy transfer over a distance ranging from 10 cm to 20 cm.
- Incorporate an MPPT (Maximum Power Point Tracking) algorithm to optimize energy transfer.
- Ensure system safety by limiting voltage outputs to 60V.
- Detect the presence of electronic loads automatically.

The development process involves creating specialized PCBs for the DC/DC converter and the DC/AC inverter, alongside executing precise efficiency assessments to guarantee optimal energy conversion.

1.3 | Challenge

The project challenges the team to craft a wireless charging solution that not only supports energy efficiency but also adapts seamlessly to both static and adjustable workspaces. The envisioned setup involves embedding a charging coil beneath the floor and another within the desktop PC, facilitating a clean and unobstructed workspace. This configuration will be rigorously tested to confirm its efficacy and reliability through various demonstrations and load tests. The setup can be seen in Figure 1.1. Please note that the image is a CHAT GPT image, which does not exactly show the configuration for this challenge. For this challenge, the coil at the PC will be situated on the outer side of the PC in a plastic compartment. This is to ensure the magnetic field is not disturbed by the metal case of the standard workspace PC.



Figure 1.1: Desk setup with wireless charging coils [7]

1.4 | Architecture

The design architecture for the wireless charging system encompasses multiple critical components:

- A generator and an AC-DC Rectifier, provided externally.
- Internally developed DC/DC Boost Converter and inverter.
- Wireless transmission coils designed for optimal energy transfer.
- A microcontroller setup to handle load detection, MPPT implementation, and dynamic control of the converters.

This comprehensive structure is designed to ensure that all parts function cohesively to meet the project's efficiency and safety requirements. Detailed documentation of each component's design rationale and performance metrics will be provided in subsequent sections of this report.

2 | System design

2.1 | General System

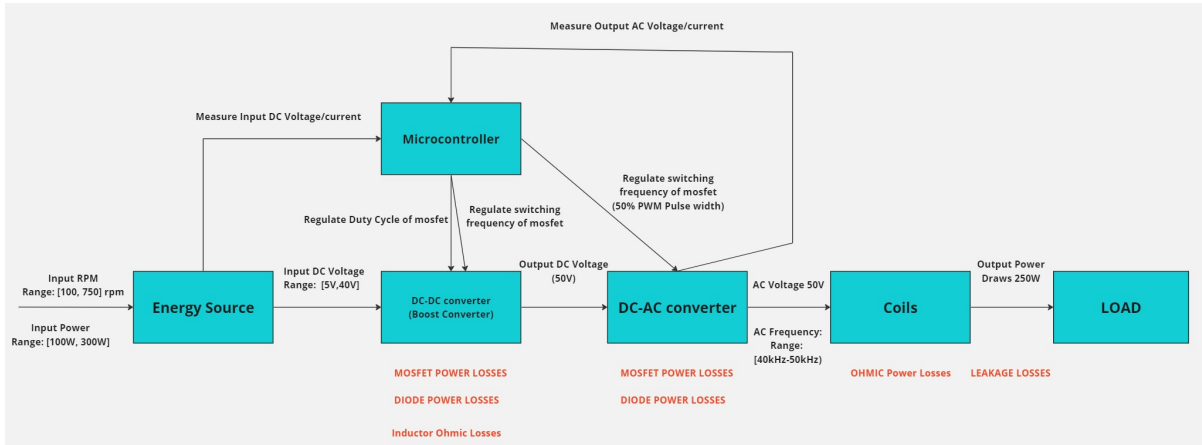


Figure 2.1: System Level Design Flowchart

In Figure 2.1, the different submodules for the project can be seen. First, the generator is configured in speed control mode and can be configured to a specific speed. This is discussed in more detail in section 3 of the report. After the generator speed is configured, the generator will output a voltage and current into the DC/DC converter. These input values will be recorded using the ADC pins of the microcontroller for further use in the MPPT algorithm, and to help in analyzing the behavior of our system. The DC/DC converter will then boost the voltage to the desired 50V voltage level. This will be done by controlling the duty cycle of the converter via the ADC pins of the microcontroller. The microcontroller will also be able to control the switching frequency of the converter, which will influence the inductor current ripple and output voltage ripple of the converter. Afterward, the new DC power will be supplied to the DC/AC in order to achieve wireless power transfer. This is because wireless power transfer requires alternating current in the primary coil, which will cause a varying magnetic flux in the secondary coil, which will result in a voltage in the secondary coil. For this to be achieved with high efficiency, a series resonance circuit will be made with a resonance frequency that matches the switching frequency of the DC/AC converter. This will be made possible by ensuring the microcontroller provides that particular frequency, and ensuring that deadtime and 50% pulse width are received by the switches of the inverter. As for the final block, the load will be the desktop PC and the characterization of the load is discussed in more detail in section 4.

3 | Energy source (Youri Lamers)

An energy source is needed to enable wireless Energy transfer to a load. A schematic overview of the energy source is shown in [Figure 3.1](#). This energy source emulates a wind generator that can generate renewable energy. A scaled-down version of the wind generator is provided by the stakeholders. The emulation of the energy source consists of three phases.

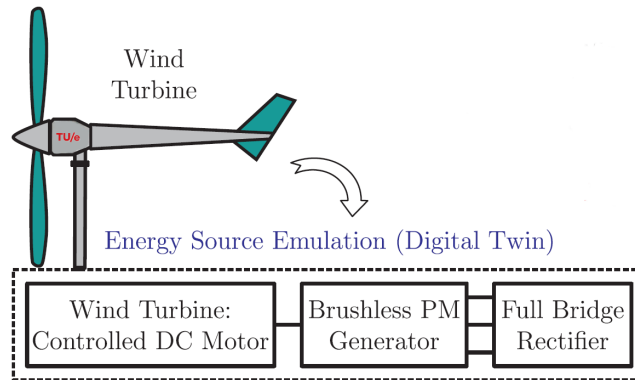


Figure 3.1: Schematic overview of the energy source [12]

The first phase consists of a wind turbine that can transform the aerodynamic torque of a wind turbine into mechanical energy by rotating a shaft [12]. This is simulated using a controlled DC motor to prevent the unpredictability of wind conditions during real-life testing [12]. The Siemens GG5104 DC motor can operate in either fixed speed or wind turbine mode. The three fixed speeds at which the overall system of [Figure 2.1](#) are tested are 250 RPM, 500 RPM, and 750 RPM.

The DC machine is directly connected via a shaft to a Hubner Giessen DSG P 7.1-07-8 three-phase brushless Permanent Magnet Synchronous machine operating in Generator mode (PMSG) [5]. The three-phase alternating current machine represents a wind generator section that can convert mechanical energy into electrical energy. An increase in wind turbine speed of the DC motor also results in an increase in voltage at the output of the PMSG. Due to the generator being an alternating current machine, the output current and voltage are also alternating. The voltage and current are afterward rectified back to DC using a three-phase full bridge rectifier which is the third phase of the energy source. The full bridge rectifier is later explained in [subsection 5.4](#).

The shaft speed and torque of the PMSG are controlled. Therefore enabling the use of operating in two different modes. Firstly, the constant speed control mode at which the DC output of the rectifier will have a constant voltage proportional to the input speed of the wind turbine. Secondly, in emulation mode, speed and torque are adjusted according to a pre-defined curve meaning that output voltage and current vary depending on the load [5]. Because of this curve, the maximum voltage does not always lead to the maximum output power of the energy source. Therefore, the point at which maximum power is achieved must be tracked to optimize efficiency. This maximum power point tracking (MPPT) will be further discussed in [section 8](#).

4 | Load (Youri Lamers)

As mentioned in [section 2](#), the load, or object that uses electric energy is a desktop PC being powered wirelessly [11]. The load emulation is the last step in the system represented in [Figure 2.1](#). Precisely describing the load type and value helps making design choices in other subsystems. A constraint is set that the load must be resistive. Therefore a research question can be asked: What is the most effective method to represent the load characteristics of a desktop PC to enable the design of the other subsystems?

The desktop PC power supply can be considered a mostly resistive load, especially when looking at operations under steady-state conditions. An accurate load value is necessary to optimize design choices regarding the energy processing subsystems. The value of this resistive load is determined using the desired voltage V_L and power P_L at the input of the desktop PC power supply. The resistor value R can therefore be given as

$$R = \frac{V_L^2}{P_L}. \quad (4.1)$$

The constraints placed for the desktop PC in [section 2](#) include $V_L = 50\text{V}$ and $P_L = 250\text{W}$. Using [Equation 4.1](#), a resistive load is obtained of $R = 10\Omega$. This load value is further used to specify and simulate the power electronic converters.

Furthermore, during testing with physical components, a provided variable slide resistor, or rheostat is used rather than through-hole resistors of the same resistance. This is due to the slide resistor's ability to dissipate significant amounts of power more limiting the chance of damaging any components [1].

5 | Power electronics

5.1 | Introduction

Ideally, the charged PC at the system's output requires a fixed voltage of 50 V. The wind turbine creates a variable output voltage and current of at most 30 V and 10 A. Therefore, the voltage must be stepped up to reach the required 50 V. A DC/DC boost converter is chosen to stabilize the varying input voltage. An AC voltage signal is used to efficiently transfer energy through the set of coils. Therefore, the DC voltage is converted into an AC voltage using a full bridge inverter.

5.2 | DC/DC Converter (Malik Weren)

5.2.1 | Introduction

The first submodule of the wireless energy transfer chain is the DC/DC converter. The DC/DC converter circuit uses power electronic devices to modify power supply waveforms in DC motor drive applications. The converter takes a rectified unregulated DC voltage as an input and converts it to a desired DC voltage level. As mentioned previously in the energy source section, the input to the DC/DC converter is a varying rectified DC voltage, which depends on the speed characteristic of the generator. For this challenge, a boost converter is chosen as research shows that DC/DC boost converters are commonly used in wireless power transfer systems to maximize power efficiency [8]. The boost converter achieves this by increasing the input voltage achieving a higher voltage on the converter's output.

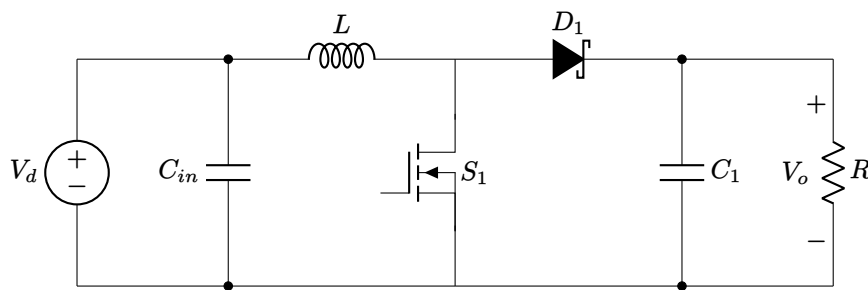


Figure 5.1: DC-DC Boost Converter Schematic

The output voltage of a DC/DC converter is regulated by adjusting the period the power MOSFET is turned on during a period. This is commonly referred to as the duty cycle. The duty cycle (D) is derived as

$$D = \frac{V_o - V_d}{V_o}, \quad (5.1)$$

where V_d is the input voltage and V_o is the output voltage. This can then be described as

$$\frac{V_o}{V_d} = \frac{1}{1 - D} \quad (5.2)$$

The boost converter circuit topology is beneficial for two main reasons. The first reason is the output power (P_o) is proportional to the square of the output voltage (V_o) as seen in this relation

$$P_o = \frac{V_o^2}{R} \quad (5.3)$$

Secondly, the output current is scaled down in the system, therefore reducing the ohmic losses of the system. However, there are two main constraints on the project: no more than 10A of current can be drawn from the generator, and the load needs to draw 50V at the output for our product. The input current I_d can be expressed as

$$I_d = \frac{1}{1 - D} I_o \quad (5.4)$$

where I_o is the output current. This would mean that for the lower input voltages, it is not possible to boost to the 50V required, and for the higher voltages, a strict duty cycle for the converter needs to be calculated to ensure the circuit input current stays below 10A.

In summary, the DC/DC converter is used for two main purposes, which are to set the output voltage of the system, and to minimize the losses in the system. The requirements of the DC/DC converter can be seen in Table 5.1. In the next section, the different design choices will be explained for the converter. This breaks down to the choice of the circuit topology type, the component selection, the switching frequency choice, and the constraint for the duty cycle. The design stage of the converter is very important to ensure the current/voltage ripple requirements of the converter are achieved, components selected will handle the currents and voltages through them, all whilst also ensuring minimal losses in the converter.

Table 5.1: Requirements DC-DC boost converter

Quantity	Symbol	Value	Unit
Switching frequency	f_s	20	kHz
Output voltage	V_o	50	V
Input voltage	V_d	5-40	V
Input current	I_d	0.33-10	A
Required power	P_o	250	W
Output voltage ripple	ΔV_o	5	%
Inductor current ripple	Δi_L	I_L	%

5.2.2 | Method

In this section, the different component/parameter design choices are split into their own sections.

Converter Topology Multiple different types of boost converters were considered for this challenge, which are the normal boost converter, normal buck-boost converter, and inverting buck-boost converter. The initial plan was to use a buck-boost converter as the buck aspect of the converter will allow our system to also be used for voltages higher than 50V at the input and meet our product's 50V standard. However, this came with many challenges. For the normal buck-boost converter, the Cuk converter was considered. The Cuk converter came with extra complexity when it comes to designing for the optimal inductance to minimize power losses, whilst ensuring low current ripple. This is because the Cuk converter makes use of two inductors for energy exchange. As for the inverting buck-boost configuration, this complexity of energy exchange is not there, but other challenges arise with this topology. The first challenge is the output voltage is inverted, so extra circuitry is needed to invert the output voltage, which will lead to more complexity and higher power losses. The second challenge is a high negative voltage is required to drive the gate of the MOSFET in this topology, which will require a high negative voltage auxiliary source. This is the reason why for this challenge, the standard boost converter is used as it is a rather simple topology, and the design alternatives had higher levels of complexity for design.

Duty Cycle One of the limitations of the generator used at the input of the converter is that it cannot supply more than 10A. The load as mentioned previously in section 4 is modelled as a 10 ohm resistor. Therefore, the output current can then be calculated as

$$I_o = \frac{V_o}{R_o} = 5A \quad (5.5)$$

Using equation (5.4), the following duty cycle equality can be derived

$$D < 0.5 \quad (5.6)$$

This would apply in the case of an ideal working system with no voltage drops through the different stages of the system. In the case of higher voltage drops in the case of the 20cm distance in this challenge, the duty cycle can be pushed up to higher levels, whilst still maintaining under 10A of input current. This constraint must be taken into consideration carefully when the converter is integrated with the microcontroller submodule.

Inductor The goal of this component is to charge up during the MOSFET's conduction and discharge to the load when the MOSFET is off. For optimal operation, the converter needs to operate in continuous conduction mode (CCM) meaning that the current ripple needs to follow this constraint

$$\Delta i_L < 2I_L \quad (5.7)$$

where Δi_L is the current ripple and I_L is the average current through the inductor. In order to ensure the circuit operates in CCM, a Δi_L equal to the average inductor current I_L is chosen to operate in CCM with a margin of 50% of I_L above the boundary condition of CCM. In order to calculate this minimum inductance value, a MATLAB script was designed to calculate the lowest inductance value needed to achieve the requirement mentioned in Table 5.1. The following MATLAB script can be seen in the Appendix. The script incremented through different input voltages and used the values mentioned in 5.1. The following derived formula was used

$$L = \frac{V_d D}{f_s \Delta i_L} = \frac{V_d D}{0.15 f_s I_L} \quad (5.8)$$

where the inductance value L can be calculated for an estimated value of the inductor current ripple Δi_L . As seen in Figure 5.2, the desired output current ripple is seen for the calculated inductor value of $100\mu H$ for the maximum current ripple situation at $V_d = 35V$. This achieves our requirement standards as seen in Table 5.2.

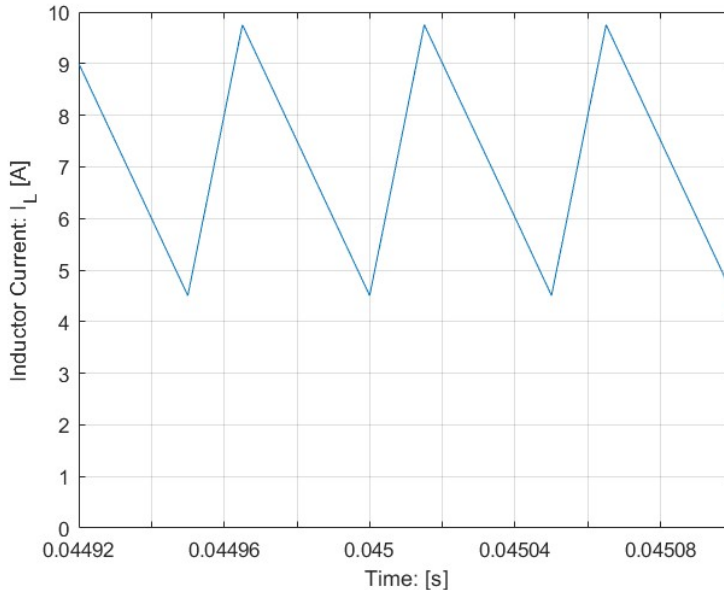


Figure 5.2: Converter Inductor Current Simulation for $V_d = 35V$ and $L = 100\mu H$

Table 5.2: Converter Inductor Current for $V_d = 35V$

Component	Avg Inductor Current	Current Ripple	Requirement
Inductor	7.13	6.92A (0.971 I_L)	I_L

Capacitor The choice of capacitance influences the voltage ripple of the output voltage (ΔV_o). The formula used for calculating the capacitance is

$$C = \frac{DV_o}{R f_s \Delta V_o} = \frac{D}{0.05 R f_s} \quad (5.9)$$

where f_s is the switching frequency of the MOSFET. Similarly to the inductor, a requirement was set for the output voltage ripple (ΔV_o) at 5% of V_o , and an estimation of the required capacitance is calculated using the same MATLAB script. The following formulas were run for a range of the possible input voltages, and the highest capacitor value calculated can be seen in Table 5.4. The chosen capacitance value then yields the following simulation graph as seen in Figure 5.3.

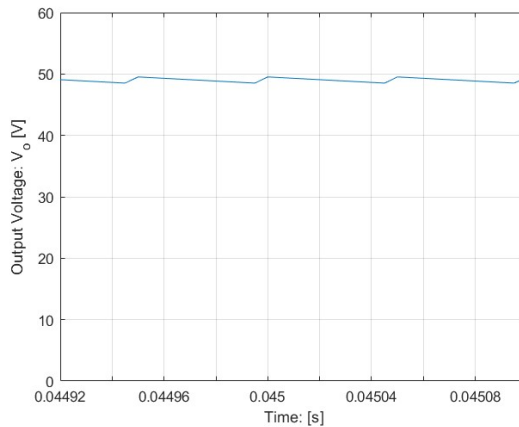


Figure 5.3: Converter Output Voltage for $V_d = 5V$ and $C = 220\mu F$

Table 5.3: Converter Output Voltage for $V_d = 5V$

Component	Avg Output Voltage	Voltage Ripple	Requirement
Capacitor	49V	2.43V (4.95%)	5%

Table 5.4: Values of Inductor/capacitor DC-DC boost converter

Component	Input Voltage	Minimum Value	Chosen Value
Inductor	35V	75uH	75uH-125uH
Capacitor	5V	90uF	220uF

Power MOSFET The power mosfet is an essential component of the circuit as it controls the charging and discharging of the inductor. It does so by controlling the flow of the current through it. For an efficient design of a DC/DC converter, it is required to consider the conduction losses and switching losses of the MOSFET. This design choice is discussed in detail in the switching frequency section. As for this section, the choice between the available MOSFETs has to be made. The two MOSFETs under consideration are the IRF630 and IRF640. When conducting simulations, the simulation shows that the benefit of using the IRF630 is the faster switching time of the MOSFET resulting in lower switching losses than the IRF640. However, the IRF640 has half the on resistance, which means that the conduction losses are 50% less. Even though both types adhere to the RMS current of this design with IRF640 handling 9A and IRF640 handling 18A as seen in Figure 5.4, the IRF640 was chosen for the final design due to its higher current threshold and considerably lower MOSFET losses due to its lower conduction losses outweighing the increase of switching losses compared to IRF630.

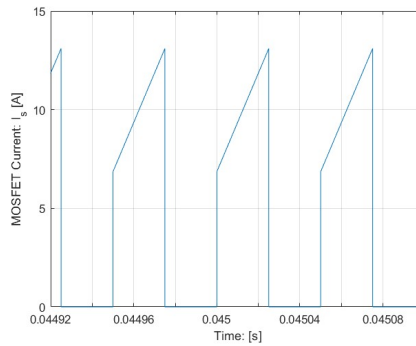


Figure 5.4: DC-DC converter MOSFET current for $V_d = 25V$

Power Diode The power diode D_1 is selected based on the diode voltage V_D and average current $I_{D,avg}$. The maximum diode voltage is equal to V_o , while $I_{D,avg}$ is given by

$$I_{D,avg} = (1 - D)I_L. \quad (5.10)$$

As mentioned previously, the duty cycle will be used around $D=0.5$ meaning the maximum current through the diode will be half of the average current through the inductor. The inductor current is the same as the input current and that can go up to 10A. This would mean that the diode should be able to handle up to 5A of current. If it is decided later on to use a lower-duty cycle, the design of the converter should accommodate that. This is why the inductor current was chosen with $D=0.20$ in mind meaning a maximum diode current of 8A. This led to the choice of using the diode model MBR10100+ with the higher-rated current at 10A as opposed to 8A of the TPS8H100D.

Gate driver This is a component used to amplify the control signal of the gate of the MOSFET. This is required to ensure the MOSFET is in saturation mode when it is conducting to ensure maximal current is charging the inductor. The low-side MOSFET driver was chosen for this circuit as the MOSFET is placed between the load and ground. The benefit of using such a gate driver as opposed to using an auxiliary power supply is the convenience it brings with controlling the signal using a microcontroller. Another benefit is its compact size in the circuit, which reduces the complexity of the circuit and provides more board space for the rest of the circuit.

Switching frequency This parameter influences heavily the losses of the MOSFET in the circuit. At the same time, the following parameter influences the current ripple and voltage ripple of the system. Therefore, a good tradeoff needs to be reached to ensure minimal losses, whilst ensuring ripple requirements are met. There are two different losses with the MOSFET. The conducting losses and switching losses. The relevant losses for switching frequency is the switching losses as the conducting losses only depend on the duty cycle of the circuit. The switching losses are defined as

$$P_{loss} = W_t f_s \quad (5.11)$$

where f_s is the switching frequency and W_t is a term that depends linearly on R_{DS} , I_D , V_{DS} , rising time, and falling time of the switch. As seen in the formula, the switching losses are directly proportional to the input current and switching frequency. For the switching frequency, the value needs to be chosen such that the converter still operates in CCM and has minor voltage ripple, whilst ensuring high efficiency of the circuit. The chosen frequency is 20kHz, which through preliminary testing proved to be optimal for higher efficiencies. This was mainly a tradeoff between using a higher switching frequency as opposed to a higher inductance. The tradeoff made would therefore be introducing more switching losses, whilst minimizing ohmic inductor losses up to a certain extent.

Table 5.5: Component list DC-DC boost converter

Component	Manufacturer and part	Description	Quantity
Electrolytic Capacitor	Panasonic EEUFC1J221S	(220 μ F, 63V)	1
Schottky Rectifier diode	Multicomp MBR10100+	(100 V, 10 A, 850 mV, TO-220AC)	1
Inductor	Epcos Not decided	-	1
Power MOSFET	Infineon IRF640NPBF	(200 V, 18 A, 0.15Ω, TO-220)	1
MOSFET Driver	Renesas EL7104CNZ	(4.5V-16V Supply, 4A, 18ns)	1
Decoupling Capacitor	Kemet C322C104K5R5TA	Ceramic Capacitor (100nF, 50V)	1

5.3 | DC/AC Converter (Jasper Kadijk)

The next step in the wireless energy transfer chain is the DC/AC converter, or 'inverter' for short. The previously discussed DC/DC converter steps the voltage level up to a level which is required to reach the desired power at the load. But before any energy can be transferred through the coils, an inverter is necessary.

The energy is transferred using the concept of inductive power transfer. Inductive power transfer uses a magnetic field to transfer electrical energy from a primary coil to a secondary coil without an electrical connection. A time-varying magnetic field produced by a current flowing through the primary coil induces a voltage across the ends of the secondary coil, according to Faraday's law of induction [3], given by

$$\epsilon = N \frac{d\phi}{dt}, \quad (5.12)$$

here ϵ is the instantaneous induced voltage, N is the number of turns and $\frac{d\phi}{dt}$ is the time-varying magnetic flux, as a result of an alternating current through the primary coil. Flux is given by

$$\phi = BA, \quad (5.13)$$

where A is the area perpendicular to the magnetic field B , which is given by

$$B = \frac{\mu_0 I}{2\pi r} \quad (5.14)$$

where one observes that the magnetic field, and thus, the flux is directly related to the current in the primary coil. The main challenge of this step in the process of wirelessly transferring energy is converting a direct current to an alternating current.

To convert a direct current to an alternating current, an inverter is used. Specifically, a full bridge inverter is being implemented, as seen in [Figure 5.5](#). This type of inverter is chosen over a half-bridge inverter because although the latter does require fewer components, the amplitude of the output voltage is half of the DC input voltage, according to

$$v_o = \frac{V_{DC}}{2}. \quad (5.15)$$

The biggest disadvantage of this in the context of this project is that the DC/DC converter would have to boost twice as much to reach the required voltage at the load.

A full bridge inverter consists of two pairs of MOSFETs. During the first half of the period, two diagonally opposite switches ($S1$ and $S4$) are switched on, and the output voltage is positive. During the other half of the switching period, the other two diagonally opposite switches ($S2$ and $S3$) are turned on, which results in the current flowing to the output in reverse polarity, and thus the voltage at the output is negative. The resulting voltage at the output is a square wave, with an amplitude equal to the input DC voltage.

Square waves are chosen at the output of the inverter, due to the reduced complexity of the circuit design compared to a pure sine wave inverter. A pure sine wave inverter employs more complex and specialized switching systems and additional filters, specifically pulse width modulation, which as the name suggests, switches rapidly and changes the width of the pulses to produce a smooth and stable waveform that approximates a pure sine wave. Besides more complex switching schemes, a pure sine wave inverter has more switching losses and higher production costs. Another consideration as to why a square wave inverter is chosen is the insignificant difference in efficiency compared to a pure sine wave inverter [2].

A simple simulation is shown in [Figure 5.6](#) to illustrate the working principle of the inverter for an input voltage of $V_d = 50$ V.

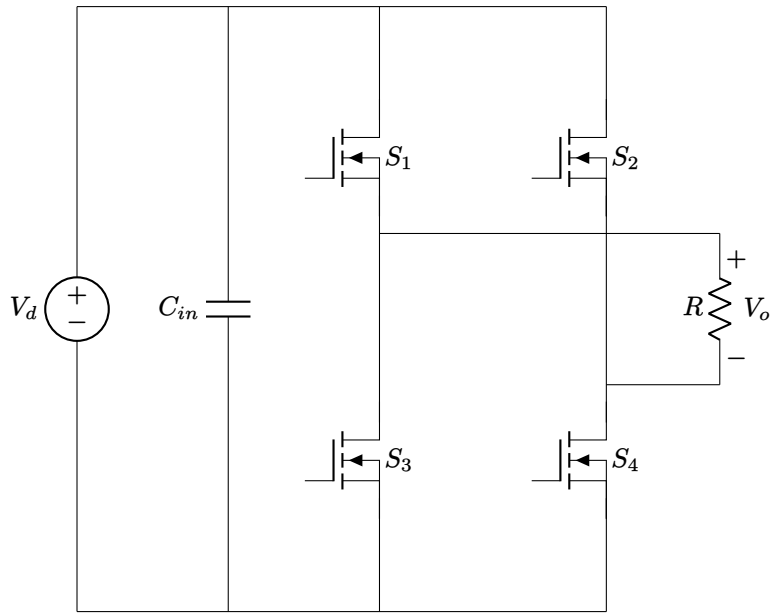


Figure 5.5: Equivalent circuit of a full bridge inverter

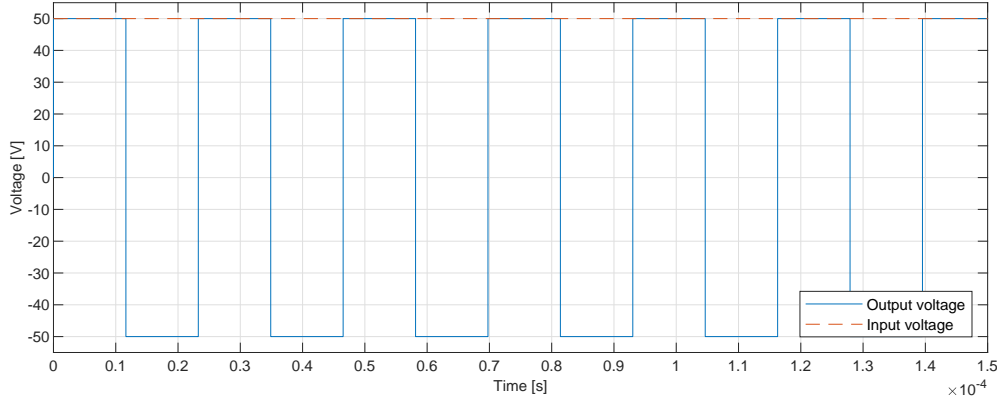


Figure 5.6: Simple simulation of a full bridge for an input of $V_i = 50$ V

As mentioned earlier, there are four MOSFETs in this circuit. Furthermore, there are two high-side and low-side drivers. These drivers can each drive two MOSFETs independently of each other. Also, there are decoupling capacitors for the main circuit and the two driver circuits to stabilize the supply voltages. A driver circuit consists of the driver, a 12 V auxiliary supply with a diode to V_B , 3 decoupling capacitors and a 3.3 V logic supply. The supply voltage is chosen to be 12 V, because the data sheet states that at 10 V or higher, the lowest on-resistance and best performance is achieved. The resistor between the output of the driver and the gate of the MOSFET has a resistance of 10 Ω . Detailed driver circuit, including all connections to the circuit and supply, is visible in [Figure C.1](#). All components are clearly stated in [Table 5.6](#).

The circuit and simulation result shown in [Figure 5.5](#) and [Figure 5.6](#) are for a resistive load at the output. Furthermore, it is purely theoretical. However, in this project, the inverter is implemented after a DC/DC converter and before a coil. These factors influence the behaviour of the inverter and this has to be taken into account in the design. The measured output of the inverter as part of the whole system, which is relevant for this part of the analysis, is shown in [Figure 5.7](#).

The first thing that has to be taken into account in the real world is dead-time. The MOSFETs that are used in the inverter are, of course, not ideal. They have a certain turn-on delay time, a rise time, a turn-off delay time and a fall time. Because the switch is not turned on or off immediately, there is a risk of a short circuit. If S_3 as seen in [Figure 5.5](#) is being switched on, while S_1 is still being switched on,

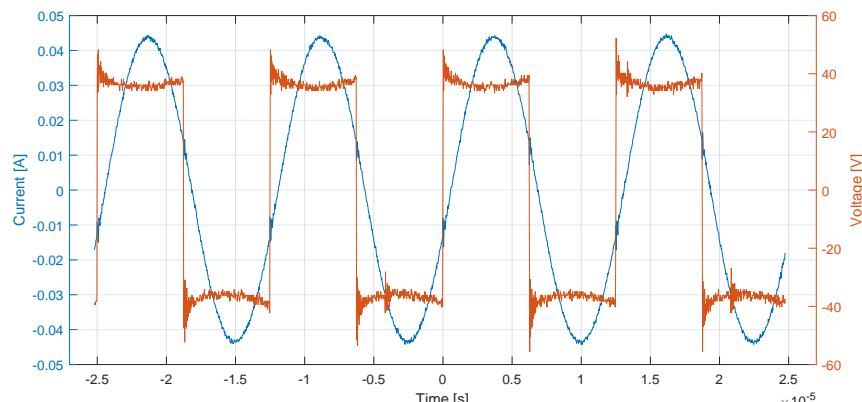
Table 5.6: Component list DC-AC inverter

Component	Manufacturer	Part number	Description	Quantity
Power MOSFET	Infineon	IRF640NPBF	Power MOSFET (200 V, 18 A, 0.15 Ω, TO-220)	4
MOSFET Driver	Infineon	IR2110PBF	High Side and Low Side	2
Decoupling Capacitor	Kemet	C322C104K5R5TA	Ceramic Capacitor (100nF, 50V)	1
Decoupling Capacitor driver	Epcos	B32529C1104K000	Plastic Film Capacitor (100 nF, 100V)	6
Gate Resistor	Multicomp	MF25 10R	Through Hole Resistor (10 Ω, 250 mW, 250 V)	4
Driver Diode	Multicomp	MBR10100+	Schottky Rectifier (100 V, 10 A, 850 mV, TO-220 AC)	2

they are both allowing current to flow from the drain to the source terminal, which causes a short circuit. To solve the problem caused by this overlap in switching times, a dead-time is introduced. This is a short period of time where both pairs of switches are turned off. In [section 8](#), the way this dead-time is calculated is explained. It depends on the specifications of the MOSFETs being used. Although dead-time is necessary for safety reasons, there are also disadvantages. Examples of these disadvantages are reduced efficiency because of the reduced effective duty cycle and harmonic distortion in the output voltage, which can lead to increased noise and ripples [\[9\]](#). Given these disadvantages, it is desirable that the dead-time is as short as possible, to minimize the effects.

As stated earlier, the inverter is connected to a coil together with a series capacitance at the output instead of a resistive load. The series capacitance is added because the capacitive impedance cancels out the inductive impedance to some extent. This allows for more current to flow through the circuit. The current in the primary coil is directly proportional to the induced voltage in the secondary coil, so this means that the power reached at the load is higher. More explanation about the series capacitance is present in [section 6](#). An effect of the magnetic circuit at the output of the inverter is the smoothing or filtering of the higher frequencies of the current, as shown in [Figure 5.7](#). In this figure, the voltage overshoot of the system is also visible. This is partially caused by the coil but also by the fast switching scheme.

By doing experiments, the behaviour of the output voltage waveform could be observed. The main focus was to check if the performance was sufficient for the requirements of the system. This implies the minimization of the overshoot and the maximization of the peak output voltage. It was found that by tilting the secondary coil approximately 10 degrees, the overshoot was less than when the coils were perfectly parallel. One could observe that as the secondary coil was tilted to some extent, the current sine wave shifted to the right and the overshoot decreased.

**Figure 5.7:** Output current and voltage of the inverter

5.4 | DC/AC Converter (Youri Lamers)

The last necessary power electronic converter is a full bridge rectifier which converts alternating voltage and current back to direct voltage and current. An AC/DC converter is used twice in the system of Figure 2.1. The first AC/DC converter is part of the energy source and is positioned right after the PMSG and contrary to the DC-DC and DC-AC converters do not have to be built. The second full bridge rectifier is placed in between the second coil and the output load. This converter is also already provided via a rectifier box [12].

Figure 5.8 shows the equivalent circuit of the full-bridge rectifier present in the rectifier box, where V_{in} represents the AC input coming from the second coil and C_o as the capacitor used as a filter to reduce voltage ripple. The specified capacitance value of $C_o = 1000\mu\text{H}$ is given. The same four Schottky diodes are represented as D . These diodes are Multicomp pro MBR16100 from supplier Farnell [10]. The load is represented by resistor R and has the same value of 10Ω .

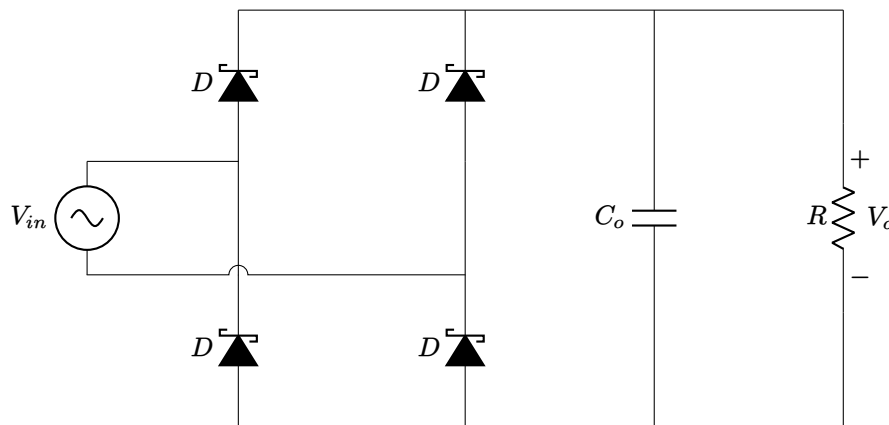


Figure 5.8: Equivalent circuit of full bridge rectifier

Figure 5.9 shows the simulated input and output voltage of the full bridge rectifier using Simulink for an input peak voltage of 50 V and frequency of 1000 Hz. The diode is simulated using MBR16100 datasheet values to give a more accurate representation. Figure 5.9 shows that the alternating input voltage V_{in} is rectified to DC output voltage V_{out} averaging 45.81V. There is still around 13.89% output voltage ripple present even with the addition of capacitor C_o .

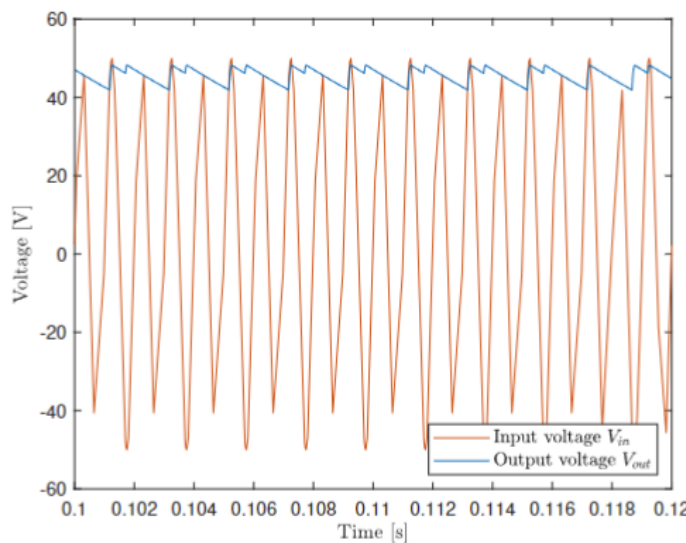


Figure 5.9: Input and output voltage of full bridge rectifier for $V_{in,peak} = 50\text{V}$, and $f = 1000\text{Hz}$.

6 | Magnetics (Radu Cretu & Codrin Danculea)

6.1 | Coil Design (Cretu Radu)

6.1.1 | Introduction

The aim of the project is to create a theoretical model and a working physical prototype of the complete system in order to implement wireless charging. This task necessitates comprehensive documentation covering all aspects of the system, including both hardware and theoretical components.

Electromagnetic induction is the method used for wireless inductive charging, which is a form of wireless power transfer. This technology has become increasingly relevant as the industry shifts towards electricity, presenting social, economic, and technological challenges that need addressing.

Wireless charging offers benefits such as enhanced convenience and reduction of physical wear on connectors by eliminating the need for contact and manual intervention during the charging process. This project focuses on developing a functional and efficient wireless charging system for a computer with a glass case, allowing the magnetic field to pass through effectively without any obstruction.

The operational principle is as follows: an alternating current supplied by the inverter flows through the primary coil, inducing a current in the secondary coil in accordance with Ampere's law. The primary and secondary coils, also referred to as the transmitter and receiver, respectively, are constructed with a flat geometry and identical configuration. This design facilitates easy alignment and maximizes coupling efficiency. The parameters of these flat coils, including their radius, number of turns, and optimal operating frequency, significantly influence the energy transfer process. Optimizing these parameters within the size constraints, while also matching the input requirements of other subsystems, is essential to achieving a sufficiently high output power with reasonable efficiency, making the coil construction critical for an effective overall system. These design choices, along with the power flow principles, will be examined in greater detail in the subsequent sections.

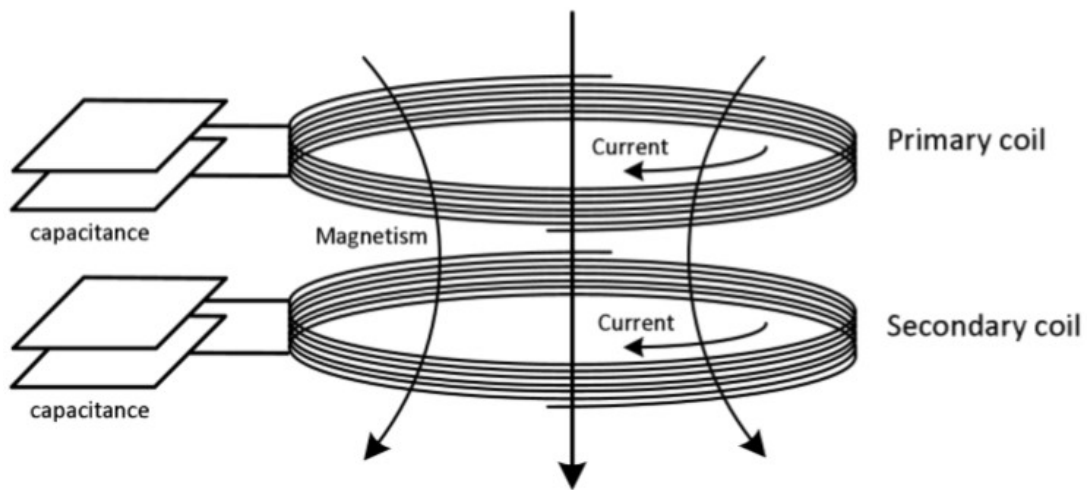


Figure 6.1: Magnetic interaction between 2 coils

The method chosen for optimizing the coil geometry is a MATLAB script that iterates through different frequencies, inner radii and numbers of turns, while also having some constants and predefined restrictions (maximum 40 cm coil diameter) given as input. The power delivered by the coil ensemble is calculated for each iteration and the efficiency is compared to the previous one in order to find the most efficient coil geometry and the optimal operating frequency of the system. Simulating the behavior of the coils for a wide range of parameters ensures a rigorous assessment and a fine-tuned design, leading to a high overall system efficiency.

6.1.2 | Coil geometry

An important design choice for manufacturing the coil is their shape and size. Flat-shaped coils facilitate alignment and are the most widespread coil geometry for wireless charging applications. Within the context of the project challenge, flat shaped coils are the easiest to fit on the side of a personal computer. With regard to the dimensions of the two coils, the coils have been chosen to have the same size. Again, this makes it easier to achieve a higher coupling coefficient since it is easier to align identical coils. Having identical transmitter and receiver coils also simplifies the calculations for the optimization process. As previously mentioned, the specifications of the coils are chosen based off of a MATLAB script that iterates through different parameters of the coils and the operating frequency. Having coils of different dimensions, would have greatly increased the runtime of the optimization script and made it harder to make adjustments as other details of the project were established.

6.1.3 | What is resonance in the context of wireless charging?

Magnetically coupled coils function similarly to a transformer but exhibit higher leakage inductance due to the larger air gap between the coils. Consequently, the fraction of magnetic coupling linking the coils is significantly smaller, classifying them as loosely coupled. To transfer sufficient power over longer distances, the system operates at its resonant frequency with a zero-phase angle between input current and voltage. The resonant frequency is the frequency at which the inductive reactance of the coils is equal to the capacitive reactance, resulting in minimized impedance and maximized power transfer efficiency. At this frequency, energy oscillates between the magnetic and electric fields with minimal loss.

The capacitive impedance, calculated using [Equation 6.5](#), largely offsets the inductive impedance, although complete cancellation is not achievable in practice. This reduction in net impedance allows for increased current flow in the circuit, applicable to both the primary and secondary sides. On the primary side, the voltage induced in the secondary side is directly proportional to the current in the primary side. Consequently, a lower impedance in the primary side results in a higher current, which in turn induces a higher voltage in the secondary side. With a lower impedance on the secondary side as well, this higher voltage facilitates an increased current flow, thereby enhancing the overall efficiency of the wireless power transfer system.

6.1.4 | Choosing a Series LC Circuit Over a Parallel LC Circuit

In the context of wireless energy transfer for personal computer charging, the Series-Series (SS) compensation network presents several advantages. By achieving resonance through precise capacitive compensation that matches the coil leakage inductance and operating frequency, SS-compensation significantly reduces impedance, thereby maximizing power transfer efficiency. Unlike SP, PS, and PP topologies, SS-compensation is less sensitive to variations in load making suitable for charging different types of computers or laptops.

The SS topology maintains high and stable transfer efficiency even when the mutual inductance is low, ensuring consistent performance. It transmits higher output power for a fixed input power compared to other topologies. This characteristic is crucial for charging personal computers, as it ensures efficient power delivery without frequent recalibration.

Using an SS-compensation network is beneficial for applications with variable load conditions, as the primary compensation capacitance remains independent of the load. In contrast, the other topologies require it to vary with load and coupling conditions, potentially compromising the resonance frequency and transfer efficiency. This independence from load variations makes SS-compensation more robust and reliable for consistent power delivery.[\[6\]](#).

6.1.5 | Minimizing impedance

In order to minimize impedance of both primary and secondary sides, the resistance has to be minimized. At high frequencies, skin effect leads to less effective conducting area within the wire and the resistance is increased. In order to minimize this effect a litz wire is used to maximize the conductive surface. With this in mind, the wire with the most strands available was the Huibers Rupalit HF Litze V155. As previously mentioned, the purpose of operating at resonance is to minimize the total impedance and have more power flow through the system. The working principle of using the compensation capacitance to achieve this is exemplified by the formulas below:

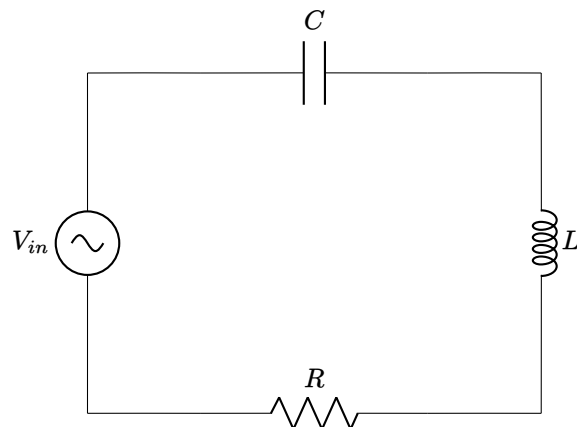


Figure 6.2: Simple Series Resonant Circuit with AC Source

■ **Capacitor Reactance:**

$$X_C = \frac{1}{2\pi f C} \quad (6.1)$$

This formula calculates the reactance of a capacitor at a given frequency f and capacitance C . Reactance impacts how capacitors impede the flow of current in AC circuits, affecting the phase and amplitude of voltage across them.

■ **Inductor Reactance:**

$$X_L = 2\pi f L \quad (6.2)$$

This determines the reactance of an inductor, which varies directly with frequency f and inductance L . It describes how inductors oppose changes in current, crucial for tuning the system's resonance.

■ **Total Impedance:**

$$Z = \sqrt{R^2 + (X_L - X_C)^2} \quad (6.3)$$

Total impedance combines resistive and reactive components, crucial for understanding how the entire circuit resists electrical flow.

■ **Minimized Impedance:**

$$Z = R \text{ (when } X_C = X_L) \quad (6.4)$$

When the inductive and capacitive reactances balance each other, impedance is minimized, optimizing power transfer by reducing losses.

■ **Capacitive Compensation:**

$$C = \frac{1}{(2\pi f_r)^2 L_{lks}} \quad (6.5)$$

This formula is used to calculate the capacitance required to achieve the resonant frequency, where the system attains maximum efficiency in power transfer. Here, the leakage inductance L_{lks} is equal to L_{lk_p} due to symmetry.

6.2 | Methods (Optimization Code) (Codrin Danculea)

6.2.1 | Model of wireless charging coils used for optimization

Designing coils for optimal power output requires both theoretical and physical models. This involves calculating coil parameters based on distance and the number of turns, and then using these in circuit simulations, to match physical model outputs. MATLAB is used for finding the optimal coil geometry, while Simulink handles circuit simulation, based on the simplified circuit in 6.3.

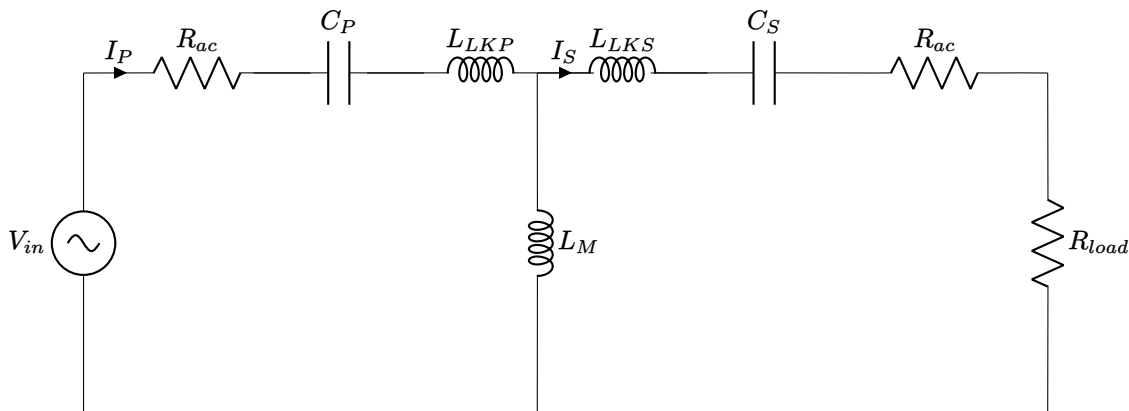


Figure 6.3: Equivalent circuit of the magnetically coupled coils

Firstly, analyze the wire specifications, including the number of strands and strand diameter, to determine the wire's actual dimensions. Additionally, calculate the wire's resistance, consisting of both DC resistance (R_{dc}) and AC resistance (R_{ac}).

Consider other geometrical parameters of the coil. By varying the number of turns and the inner radius, different configurations can be tested to achieve optimal performance. The inner radius and number of turns may result in a higher transmitted flux but will result in more resistance and ohmic losses. At the same time, a higher frequency will generate a greater voltage in the secondary side as demonstrated by equation (6.12), but will lead to increasingly high skin effect losses according to equations 6.7 - 6.2.3. These considerations are further detailed upon in the optimization script subsection.

Finally, with the chosen inner radius and number of turns, the outer radius of the coil is computed such as to assure that it is under the required dimension. The MATLAB script developed for this project aims to optimize coil parameters for a wireless power transfer system, focusing on maximizing efficiency and ensuring sufficient power delivery to the load, a minimum of 100W. This subsection describes the mathematical formulas used in the script and explains their significance in the optimization process. For the sake of simplicity, the coils have been assumed to be symmetrical from the beginning, in order to simplify the calculations and complexity of the system, having an equal number of turns and inner radius.

6.2.2 | Initialization

The MATLAB script initializes by defining essential constants necessary for the calculations. These include physical properties such as the permeability of free space and the resistivity of copper. The ranges for adjustable parameters like the number of turns, inner radius, and frequency are also set up here. The script iterates over the three aforementioned parameters in small increments, in order to assure that the optimal combination is properly represented. For each iteration, the efficiency is calculated using the given parameters, and if a better efficiency value is found, the optimal parameters are updated. The chosen ranges for the optimization parameters are as follows:

- Number of turns: 10 - 30
- Inner radius: 0.1 - 0.25 m
- Frequency: 40,000 - 80,000 Hz

This initialization process ensures that all necessary constants and parameter ranges are defined before the optimization begins, allowing the script to find the optimal combination of coil parameters, thereby maximizing the efficiency of the wireless power transfer system while ensuring that the size constraint of 40 cm is met and also that sufficient power delivery to the load, namely at least 100W at 10 cm, since maximal efficiency is the goal of the magnetics subsystem.

6.2.3 | Formulas Used in Calculations

This section integrates critical formulas within the optimization loop, enabling dynamic parameter adjustments based on computed outcomes.

Coil Geometry and Resistance Calculation

■ Turn Length:

$$l_{turn} = (R_{in} + R_{out})\pi \quad (6.6)$$

Determines the length of one complete turn of the coil, essential for calculating the wire's resistance.

■ Skin Depth and Correction Factor:

$$\delta = \sqrt{\frac{\rho}{\pi f \mu_0 \mu_r}} \quad (6.7)$$

$$k_s = \begin{cases} 1 & \text{for } \delta \geq r_s, \\ \frac{\delta}{r_s} & \text{for } \delta < r_s. \end{cases} \quad (6.8)$$

Skin depth affects the effective resistance of the wire at high frequencies by reducing the conducting cross-sectional area. The correction factor adjusts resistance calculations accordingly.

■ DC and AC Resistance:

$$R_{dc} = \frac{4l_{turn}}{\pi d^2 n^2 k_s}. \quad (6.9)$$

$$R_{ac} = R_{dc}(1 + \gamma_s). \quad (6.10)$$

Direct current resistance is calculated first, and alternating current resistance is adjusted for the proximity effect, which accounts for non-uniform current distribution due to adjacent conductors.

■ Proximity Effect Factor:

$$\gamma_s = \frac{\pi^2 f^2 10^{-14}}{3R_{dc}^2 + \pi^2 f^2 10^{-14}}. \quad (6.11)$$

This factor quantifies additional losses in AC systems, enhancing the accuracy of resistance calculations.

Mutual Inductance Calculation

Mutual inductance is a crucial parameter in the design of wireless charging coils. It quantifies the coupling between the primary and secondary coils. The mutual inductance (M) can be calculated using the following formula:

$$M = \frac{V_s}{2\pi f I_p} \quad (6.12)$$

This is useful for calculating the mutual inductance of the manufactured coils, while in the optimization code the mutual inductance is approximated using a function that calculates the magnetic flux through one coil due to the current in another coil. The function iterates over the number of turns and calculates the flux density using the FLUXDENS function. Specifically, the function initializes variables for radius and flux and sets a step size for the radius segments of the primary coil. For each combination of turns, it calls the FLUXDENS function, which iterates through the steps of the surface of the entire coil, to obtain the magnetic flux density and the corresponding radius values of the secondary coil. Within a nested loop, it calculates the magnetic flux for each radial segment by summing the product of the flux density and the area of the annular segment. Finally, the total flux is divided by the source current to determine the mutual inductance, providing a numerical approximation based on the physical dimensions and electrical properties of the coils. This method ensures an accurate estimation of mutual inductance, essential for optimizing coil performance.

Leakage Inductance Calculation

Leakage inductance represents the portion of the magnetic flux that does not contribute to energy transfer between the primary and secondary coils, which should eventually be cancelled out by adding the capacitance. The leakage inductance for the primary (L_{lkp}) and secondary (L_{lks}) coils can be calculated using the following formulas:

$$L_{lkp} = L_p - M, \quad L_{lks} = L_s - M \quad (6.13)$$

The leakage inductance of each coil

Where:

- L_p and L_s are the self-inductances of the primary and secondary coils, respectively.
- M is the mutual inductance.

Output power and efficiency evaluation

The script calculates output power, input power, and efficiency for each configuration, identifying the optimal parameters that yield the highest efficiency. The results guide the physical prototype development and further theoretical model adjustments.

These detailed calculations ensure the designed system is both efficient and effective for the intended application, with systematic adjustments and real-time evaluation of coil design parameters.

At the resonant frequency (f_r), the leakage inductances L_{lks} and L_{lkp} are equal. To counteract the effects of leakage inductance, capacitors are added to the circuit. These capacitors create a resonant circuit that cancels out the reactive effects of the leakage inductance, thus optimizing the power transfer efficiency. With the calculated leakage inductances and the mutual inductance, their impedance in the circuit model can be obtained:

$$Z_{L_{lkp}} = j\omega L_{lkp}, \quad Z_{L_{lks}} = j\omega L_{lks}, \quad Z_{L_m} = j\omega M \quad (6.14)$$

The same goes for the compensation capacitances

$$Z_{C_s} = \frac{1}{j\omega C_s}, \quad Z_{C_p} = \frac{1}{j\omega C_p} \quad (6.15)$$

The total impedance of the secondary side and the mutual impedance in parallel can be obtained:

$$Z_{eq} = \frac{Z_{L_m}(Z_{L_{lks}} + R_{ac_{tot}} + Z_{load} + Z_{C_s})}{Z_{L_m} + Z_{L_{lks}} + R_{ac_{tot}} + Z_{load} + Z_{C_s}} \quad (6.16)$$

Then, using a voltage divider, the secondary voltage is calculated with

$$V_s = V_{in} \frac{Z_s}{R_{ac_{tot}} + Z_{L_{lkp}} + Z_{C_p} + Z_s} \quad (6.17)$$

Having calculated the secondary side voltage and knowing the input voltage, both the primary and the secondary currents can be calculated:

$$I_s = \frac{V_1}{Z_{L_{lks}} + Z_{C_s} + R_{ac_{tot}} + Z_{load}} \quad (6.18)$$

$$I_p = \frac{V_{in}}{R_{ac_{tot}} + Z_{L_{lkp}} + Z_{C_p} + Z_1} \quad (6.19)$$

From these equations it can be seen how at resonance, if the leakage inductance impedance and compensation capacitor impedance cancel each other out it will lead to a higher current both in the primary and the secondary sides. Knowing all voltage and current values the power transmitted by the coils can be calculated:

$$\eta = \frac{V_s \cdot I_s}{V_{in} \cdot I_p} \quad (6.20)$$

6.3 | Optimization Results (Codrin Danculea)

The results obtained from the MATLAB optimization script provide critical insights into the effectiveness of the proposed coil designs for wireless power transfer. This section presents the findings, including optimized parameters, efficiency metrics, parameters of the coil itself, and compares these results against the project objectives. They can also be compared to measured quantities of the coils, namely self inductance, mutual inductance and AC-resistance.

6.3.1 | Optimization Outcomes

The MATLAB script identified coil configurations that maximize efficiency while ensuring sufficient power transfer. The optimized parameters, which include the number of turns, coil radius, and operating frequency, were determined based on their ability to enhance the system's overall performance, with the script having predicted an efficiency of 88.4 %. The obtained efficiency is consistent with the simulink prediction for the coils from [Table 9.1](#).

- **Number of Turns:** The chosen number of turns is 20, balancing inductance and resistance effectively, optimizing the reactance for the desired frequency.
- **Inner Radius:** The inner radius of the coils is set to 17 cm, demonstrating a significant impact on the magnetic field distribution and efficiency.
- **Operating Frequency:** The operating frequency is set to 80 kHz, which is the maximum frequency that was indicated by the power electronics subgroup. This implies that the skin effect losses were not high enough to offset the advantage offered by having a higher mutual inductance at higher frequencies.

6.4 | Coil Parameters (Cretu Radu)

The validity of the script can be verified by comparing values in the script with real-world measurements of the manufactured coils. The self inductance and resistance of the coils have been measured with an impedance analyzer. The mutual inductance was calculated using [Equation 6.12](#) after the primary current and secondary voltage of the coils connected to an AC power source were measured with the use of an oscilloscope. These results are compared in [Table 6.1](#).

Table 6.1: Optimized and Measured Coil Parameters

Parameter	Optimized Value	Measured Value	Relative Error (%)
Self Inductance (μH)	306	304	0.65%
Mutual Inductance (10 cm) (μH)	88.777	73.148	17.60%
Leakage Inductance (μH)	217.22	229.85	5.81%
AC Resistance ($\text{m}\Omega$)	504.8	420	16.80%

The close alignment between the measured and calculated values confirms the accuracy of our simulation methods and manufacturing processes. These parameters are critical for achieving the desired efficiency and performance in wireless power transfer applications.

With the coils manufactured and tested, the final specifications are determined and the subsystem can be integrated into the whole setup. The optimized coil dimensions and the measured parameters are displayed in table [Table 6.2](#).

Table 6.2: Parameters for the coils at 10 cm height

Parameter	Symbol	Value
Number of turns	N	20
Inner radius	R_{in}	17 cm
Outer radius	R_{out}	20 cm
Self inductance	L	304 μH
Mutual inductance	L_m	73.148 μH
Leakage inductance	L_k	229.85 μH
Resonant capacitance	C_k	16.3 nF
Operating frequency	f	80 kHz
AC resistance	R_{ac}	420 m Ω

6.4.1 | Comparison with Project Objectives

The results confirm that the project objectives have been met. The optimization process successfully led to the development of a system capable of efficiently transferring 100W of power wirelessly. This robust design demonstrates scalability for larger applications and adaptability for more specialized use cases, showcasing the potential for further advancements and practical implementations.

6.4.2 | Future Work

While the current results are promising, there are several avenues for further research that university students can explore to enhance the wireless power transfer system:

- **Using Primary and Secondary Coils of Different Dimensions:** Experiment with primary and secondary coils of varying sizes and shapes. This could help identify configurations that maximize power transfer efficiency and adaptability to different device requirements.
- **Increasing Iteration Steps in MATLAB Code:** Enhance the optimization script by increasing the number of iteration steps. This will allow for a more granular search of the parameter space, potentially leading to more efficient coil designs and better overall system performance.
- **Optimizing Placement and Alignment:** Study the effects of coil placement and alignment on power transfer efficiency. This includes experimenting with different distances and angles between the coils to find the optimal configuration for various applications.
- **Implementing Adaptive Tuning:** Develop and test adaptive tuning mechanisms that adjust the operating frequency or coil parameters in real-time to maintain optimal performance under varying load conditions.
- **Simulating Environmental Factors:** Use simulations to understand how environmental factors, such as temperature variations and electromagnetic interference, affect the system's performance. This can lead to the development of more robust designs.

These research directions will help refine the system's design, ensure its applicability in real-world scenarios, and provide valuable hands-on experience for university students.

6.5 | Conclusion (Codrin Danculea)

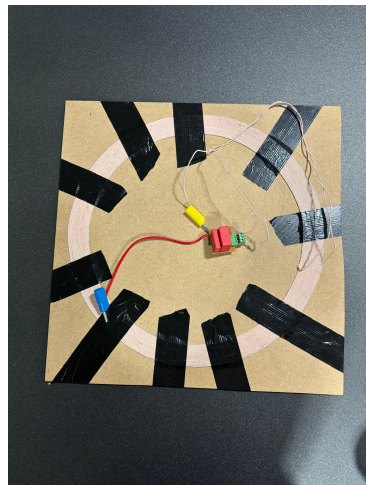


Figure 6.4: Manufactured coils

The MATLAB optimization script has proven to be a valuable tool in designing a high-efficiency wireless power transfer coils. The application of theoretical principles and detailed simulations has enabled the system to successfully reach the target of 100W and achieve good predictions for power transmitted at different distances and generator speeds. The coil measurements were compared to parameters outputted by the script and have been deemed to be accurate.

7 | PCB Design

Several vital limitations and considerations were addressed in designing both the PCBs.

First, size limitations dictated by requirements were accounted for, and the general shape of the PCB was outlined.

The most important of these was dissipation. Two separate practices were taken to manage this problem: using the ground node as a heat sink made it cover almost all of the possible surface area on the bottom side of the PCBs, and secondly, accounting for heat sink dimensions and their installation.

Another critical factor was to ensure that all the PCBs could handle the power in use. To satisfy this requirement, each PCB's power track would be thickened to direct about 9A with an allowed rise in temperature of 40°C. It was also ensured that, as general good practice in designing the PCBs, capacitors were placed as close as possible to the needed terminals of components; tracks that may differ potentially were accounted for; and "connection terminals" were placed at easy-to-access places.

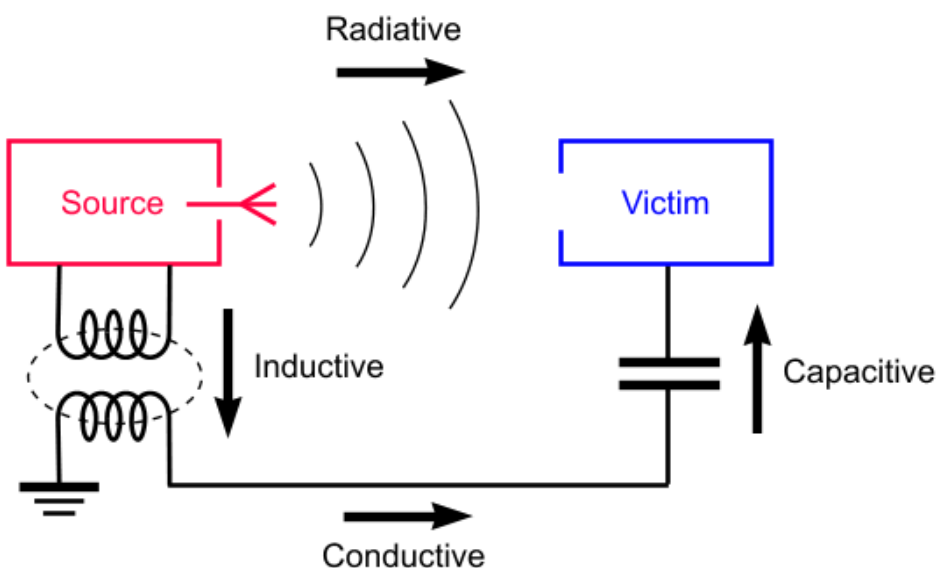


Figure 7.1: The four electromagnetic interference modules. Source: [4]

7.1 | DC/DC design choices (Daniel Tyukov)

7.1.1 | Introduction

The first system in the row of subsystems that make up the wireless energy transfer project is, therefore, a DC/DC boost converter PCB. Since this part follows in the generator and voltage rectifier, probable oscillations or noise values in the incoming power must be accounted for. Primary objectives were set with respect to ensuring robust performance against potential interference, ensuring low electromagnetic interference, and efficient thermal dissipation management.

Since there was the risk of oscillations in the generator's output, design practices had to be included to ensure the stability and reliability of the DC/DC conversion process. Current sensors were also planned initially to be installed to monitor the currents and determine maximum power point tracking but with the initial wrong assumption of two current sensors being required this was later rectified and changed to one.

The research questions that were the primary objective during the whole PCB design procedure were the following:

1. Have the best practices for PCB Design focusing on EMC and Heat dissipation been utilized?
2. How will the DC/DC subsection be utilized for the final working system and what will be the changes after the design stage?

7.1.2 | Schematic Design

The design process started with translating the DC/DC converter schematic into KiCad. This was done by selecting components that would work with various parameters under plan and specification. Placeholders for a couple of capacitors and resistors had been placed in the initial schematic to make the design flexible.

Although at the time of designing this schematic, the values of the decoupling and bypass capacitors were not fixed, general capacitors were placed at strategic positions. Also, in the case of resistors used for voltage dividers, unlike providing their exact resistor values, representing them as ratios gave room for later modification.

The inductor was connected externally with the terminal header blocks to save space on the PCB. Addition of an LED for monitoring the operational status of the system and incorporation of several terminal headers to make measurement easy at critical points on the PCB incorporated. [7.5](#)

Later on the components were chosen to be retrofitted to the designed PCB: The components selected for the schematic include:

- 4 double screw-in connectors
- 2 triple screw-in connectors
- 2 current sensors (later on discarded to one)
- 1 EL7104CNZ IC
- 1 IRF640NPBF MOSFET
- 9 capacitors ($0.1 \mu F$)
- 2 resistors (100Ω)
- 2 resistors (10Ω)
- 2 resistors ($20 k\Omega$)
- 2 resistors ($1 k\Omega$)
- 1 MBR10100+ diode
- 1 LED
- 1 capacitor ($220 \mu F$)

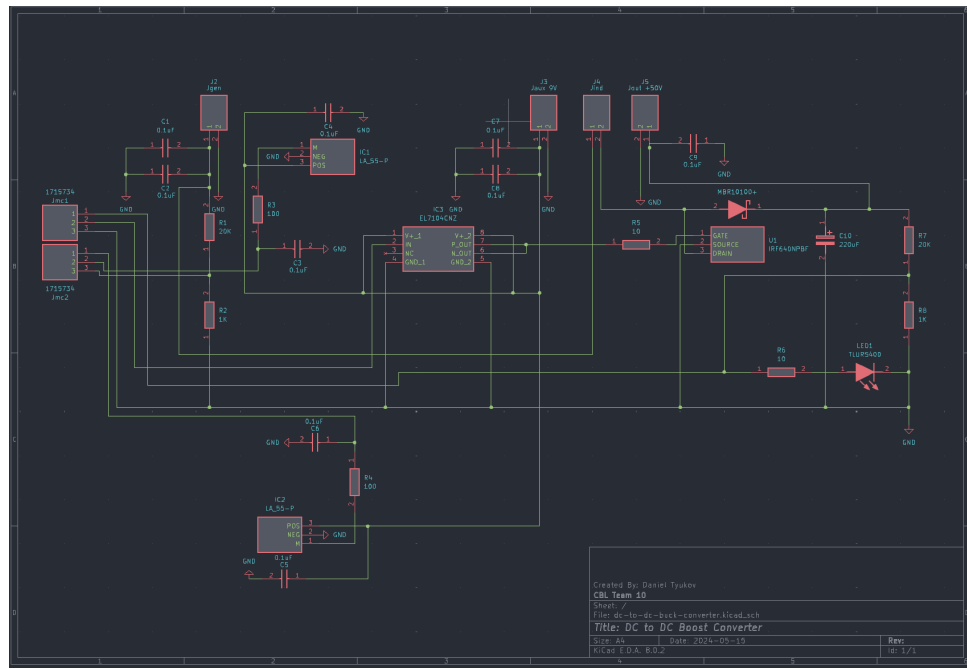


Figure 7.2: PCB Schematic of the DC to DC Boost Converter

7.1.3 | Layout

The next task was to determine the physical layout, which would involve the selection of appropriate footprints for every component and then laying these out to optimize the design for performance on the one hand and manufacturability on the other. Crossing over the ground plane with power traces would not be good, so wherever possible, that was tried to avoid cross-hatching with the ground plane to minimize potential EMI issues. [7.6](#)

Key aspects of the layout included:

- **Component Placement:** Ensuring that heat-generating components were placed for maximum airflow and heat dissipation. Those components with significant power dissipation have been located so as not to create hotspots allowing efficient thermal management.
- **Trace Widths:** The traces were sized after determining with a PCB trace width calculator the widths required to carry the expected currents without excessive heating. Wider traces and copper pours were used for high-current paths.
- **Ground and Power Planes:** Continual ground planes and separate power planes were used to minimize noise and crosstalk. High-frequency signals were carefully routed to avoid interference.

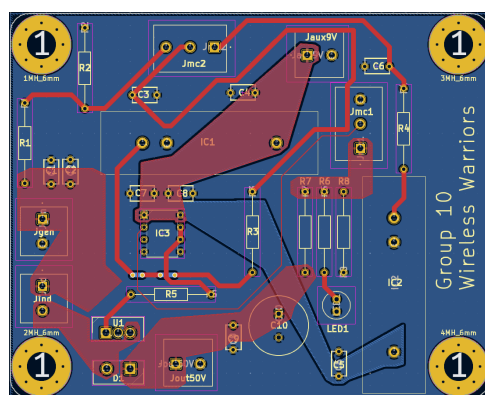


Figure 7.3: PCB Design Layout of the DC to DC Boost Converter

7.1.4 | Assembly and Testing

The last part was the assembling and testing of the PCB. It involved soldering all devices on the PCB and rigorously testing them to ensure they worked according to the desired features. Several problems were encountered and overcome during assembly.

The footprint for diode D1 did not match this component. This meant that modification was required by way of bending the legs of the diode to match the through holes. Initial capacitor placement of C1, C2, and C9 was not conducive to proper power flow. The capacitors C1 and C2 were relocated closer to the input terminal block; altogether, there was no need for capacitor C9. The values taken for the resistors in the voltage dividers were incorrect. These were altered by the practical testing.

After testing, the following additional issues were discovered:

The series resistor R6 and the LED interfered with the voltage divider and had to be removed. The misassumption of two current sensors being required for the DC/DC design for sensing the current at the input and the output at two separately for the algorithm was corrected by simply not using the spot for the other current sensor.

Finally, after addressing these issues, the PCB worked based on the specifications. It exhibited relatively stable temperatures with no hot spots and proved signal integrity through its stable and reliable operation. The last test phase was to integrate this DC/DC boost converter PCB with the overall wireless energy transfer system. It can be said that the performance of this PCB was acceptable because it efficiently boosted the voltage, and its output end was stable for the following stages. Modifications and optimizations, taken care of during all the phases of assembly and testing, guaranteed a reliable operation of the PCB within the system. [7.4](#)

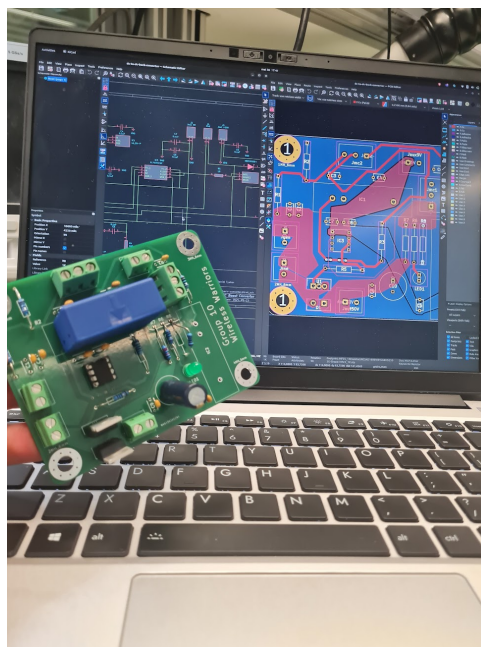


Figure 7.4: PCB Physical Layout of the DC to DC Boost Converter

7.1.5 | Reduction of Electromagnetic Interference (EMI)

EMI minimization forms a very big part of ensuring reliable operations of the DC/DC Boost Converter, particularly in such sensitive electronic equipment. The following measures were taken to minimize EMI:

- **Ground Plane Implementation:** A continuous ground plane was used for providing a low-impedance return path to the power and signal traces, reducing noise, crosstalk, and interference by shielding the signal traces from other circuits and reducing the loop area.
- **Decoupling Capacitors:** The decoupling capacitors were located near the power supply pins of ICs to absorb noise and stabilize voltage. Parallel combinations of these capacitors with larger bypass capacitors ensure low impedance over an extensive frequency range.

- **Minimized Loop Areas:** This is ensured by reducing the high-frequency loops to a minimum size to avoid voltage spikes, ringing, and noise. This is accomplished by keeping decoupling capacitors as close as possible to their ICs of interest, together with optimization of the routing for high-current paths.
- **Use of EMI Filters:** EMI filters were introduced into the PCB design to reject unwanted high-frequency signals. Low-pass filters were made use of in allowing low-frequency signals to pass and attenuating the high-frequency noise.

7.1.6 | Thermal Management

An effective thermal management system was needed to ensure the reliability of the DC/DC Boost Converter:

- **Optimized Trace Width:** The width of the copper traces was calculated to handle the expected current without overheating and within constraints using an online PCB trace width calculator. Also, more considerable traces and copper pours were used for high-current paths to reduce resistance and generate heat.
- **Heatsink for MOSFETs:** Given proper handling of dissipation, heatsinks were provided for the MOSFETs. With heatsinks attached to the MOSFET devices, the developed heat will get conducted away from the device and fanned out in the air; therefore, it will not overheat and ensure reliable operation under high power conditions.
- **Thermal Vias:** The intention was to conduct heat from the top layer of the PCB to the bottom layer and dissipate it effectively by using thermal vias. This technique helps spread the heat over a larger area, reducing hotspot formation.
- **Avoiding 45° Angles:** Also, the PCB design avoided using more than 45° angles in traces and planes. Such angles can result in crowding of the current, which increases both heating and problems related to EMI.
- **Component Placement:** All the heat-generating components were placed to allow optimal airflow and create an efficient cooling system. Keypoints Those components that dissipate more power were then placed in well-ventilated areas and away from temperature-sensitive components.

7.1.7 | Conclusion

Addressing the research questions well, the DC/DC PCB design was concluded. In developing the PCB design, it focused on specific best practices while considering EMI reduction and thermal performance management. After some struggle to assemble the board and place the first components in their correct positions, the result of the PCB design fulfilled all of the mission requirements specified and fitted well into the system as a whole.

These efforts guaranteed the demonstration of wireless energy transfer and thus validated the design choices made in the process. Adjustment and improvement during the testing contributed to a robust and reliable DC/DC Boost Converter that enhanced the whole system's performance.

7.2 | DC/AC design choices (Martin Genchev)

7.2.1 | Introduction

The second stage of the wireless energy transfer project is the DC/AC full bridge converter PCB. Its purpose is to create a square wave out of the incoming DC constant voltage from the DC/DC converter that is subsequently filtered by the LC low pass filter created by external capacitor bank and the coil itself. Several inputs must be provided externally to the PCB for it to function properly - main power/auxiliary power supply and PWM signals from the micro-controller. Following the same primary design objectives from the DC/DC PCB, it was crucial to ensure low electromagnetic interference and efficient thermal dissipation.

The research questions that were a primary objective in the PCB design procedure were the following:

1. Have the best practices for PCB Design focusing on heat dissipation and manufacturing
2. The DC/AC as a discrete component by itself and its following integration in the system as a whole
3. Decoupled modular design, that allows for easier debugging

7.2.2 | Schematic Design

Similarly to the DC/DC, the DC/AC converter schematic was translated into KiCad. Several complications arose during that process, mainly lack of preset symbols and footprints and subsequently their organization. The operation of the converter did not require any specific resistors nor capacitors, so placeholder elements for both were used, whilst all capacitors were chosen to be 100nF.

List of all components used for the PCB (excluding measurement circuits):

- 6 double screw-in connectors
- 2 110-87-314-41-001101 IC sockets
- 2 IR2110PBF MOSFET DRIVER
- 2 MBR10100+ POWER DIODES
- 4 IRF640NPBF MOSFET
- 5 capacitors ($0.1 \mu F / 100V$)
- 4 resistors (10Ω)

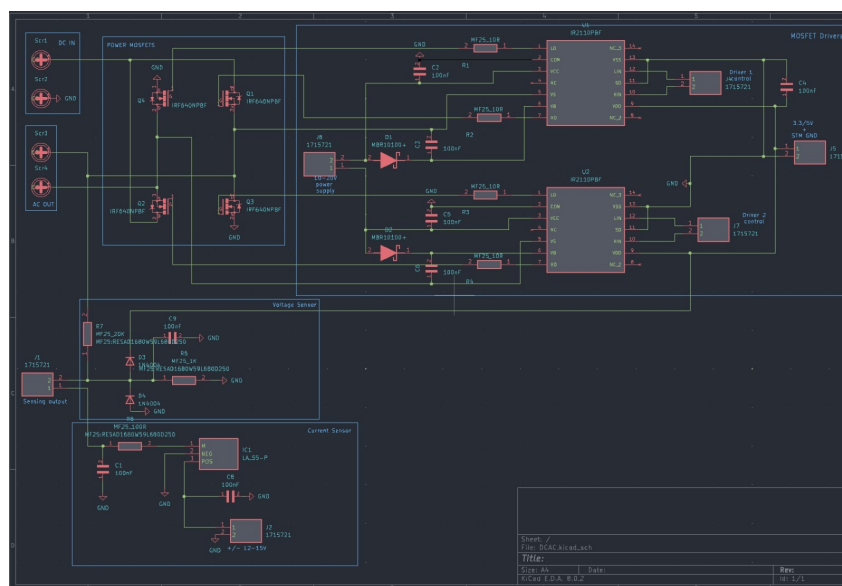


Figure 7.5: PCB Design Layout of the DC to AC

7.2.3 | Layout

After completion, the schematic design was moved to the creation of the physical PCB. However, before doing anything, several procedures had to be performed to ensure functionality of the PCB. Those were ensuring every component has its proper footprint, calculating the track length needed for the PCB to not overheat and allocating space so the MOSFET heat-sinks can be physically installed.

For the tracks width, it was separated between 3 levels based on current requirement - signal, auxiliary and main power.

- 1. Main Power** It was calculated using the Electrodoc calculator for 40°C of allowed temperature rise at 9A of current. The tool suggested 2.68mm (105.6mil) width. Due to limitations, the thickness used was lowered to 2.5mm.
- 2. Auxiliary** to support the needed current of the MOSFET drivers - 1mm trace width
- 3. Signal** The default track width of KiCad was used

During the planning of the PCB it was assumed that it will need its own current and voltage sensors, so those measurement circuits were added onto it. During the following weeks of the project it was however concluded that they were not needed and so were disregarded. Additionally, it was assumed that the main power will run through the screws that connect the DC/DC and the DC/AC PCBs, so this is the reason why for the main power input and output of the PCB the power terminals are the mounting holes. Interference is always present in electronics, so design practices to limit their effect on the function of the PCB were employed. This took form in capacitors, in close proximity to crucial components, between different nodes and ground and diodes to control current.

During the design phase of the converter, there were several uncertainties about its connection to the rest of the system. To account for such variations and to additionally ease bug testing, some inputs are repeating themselves. For example, the PWM signals from the micro-controller can be isolated, so only one of the drivers is functional at a given moment.

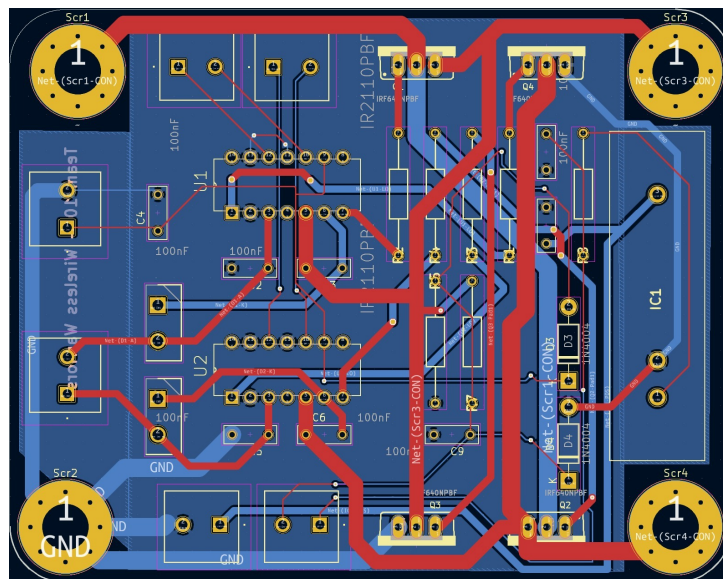


Figure 7.6: PCB Schematic of the DC to AC

7.2.4 | Assembly and Testing

Initially, the PCB was tested to verify all connections to external inputs were correct. Afterwards it was connected to the whole system and no major malfunctions occurred.

The testing and assembly phase of the project showed one big flaw of the DC/AC PCB, which is the self-inductance of the main power lines. This was caused by the relatively large distance between the individual MOSFETs and the surrounding circuitry. This was partly fixed by installing capacitors between the bridges to lower the self-inductance of the tracks.

Furthermore, upon installing the MOSFETs, it became apparent that the allocated space for the heat-sinks

was not enough. This was solved by drilling an additional hole through the body of the heat-sink and using one per two MOSFETs.

7.2.5 | Thermal Management

Overall, the main concern of the DC/AC in regards to the thermal management was the MOSFET heat-sinks. It was calculated that through an individual MOSFET, during maximum operational power levels, it would consume approximately 11W. This, combined with the aforementioned fitting of the heat-sinks, resulted in the choice of the TV40G heat-sink, which is the best available one.

7.2.6 | Areas of improvement

Due to the short limited time that was allocated for the design of the DC/AC converter, there are some additional design flaws that did not affect the operation of the converter.

Such one flaw is the overuse of the two pin terminals, which could have been easily replaced by one big common terminal.

7.2.7 | Conclusion

The DC/AC converter PCB design addressed well all the research questions. Even with all mentioned possible improvements, when it was connected during the extensive testing phase it proved to be a reliable component of the system and did not reach any critical points that could lead to malfunction.

8 | Microcontroller (Ben Lentschig)

8.1 | Feedback loop principle

The main idea behind the microcontroller is not only to drive the transistors used to act as switches, but also to control the feedback loop required to adjust duty-cycles of said transistors for varying inputs of voltage and current. To do so, the microcontroller outputs PWM signals with a signal swing of 0 to 3.3V at a certain frequency and duty cycle. These PWM signals are adjusted according to the measured voltages and currents via the microcontroller's ADC pins, allowing for real time feedback loops. Important to consider are the sink current, source current, input and output voltages of the microcontroller, which require additional resistances for it to read currents or voltages in higher ranges than 0 to its maximum sink current. Not only is the microcontroller used to set duty-cycles but also to fine-tune the switching frequencies of the converters, which can affect overall system efficiency. For this implementation, one microcontroller is utilized, which controls both circuits simultaneously. Although this stresses the microcontroller more, this allows for easier and instant communication between the DC/DC and DC/AC instead of using USART with 2 microcontrollers.

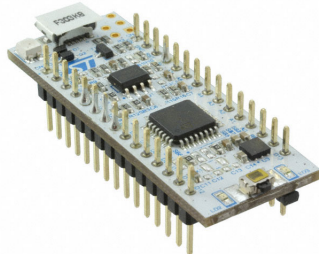


Figure 8.1: STM32 F303K8 - Microcontroller

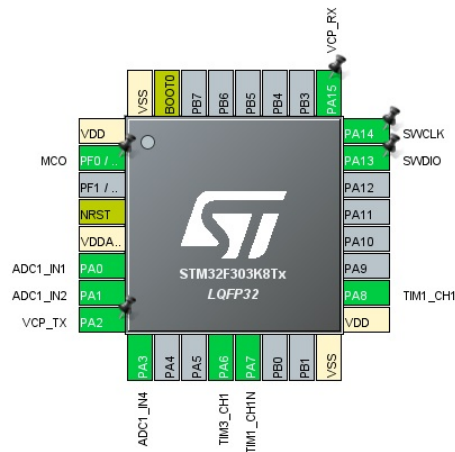


Figure 8.2: Configured pins of the f303k8

8.2 | Nucleo-32 F303k8 Board details

The microcontroller used for this feedback loop is seen in Figure 8.1, is the Nucleo- 32 F303k8, using a STM32F303K8 MCU that features a floating point unit, 32-pin package, customizable I/O pins, and pre-installed HAL library. Important to consider is the Appendix A with all tolerances, each pin and the total sum of pins used have a limit on voltage and current in/out which have to be accounted for.

8.3 | Timer and ADC configurations

The f303k8 board has several configurations for its peripherals such as timers and ADCs. The timers were kept basic, using the internal system clock H_{CLK} at 64Mhz, which is not its maximum of 72 Mhz, the timers' speeds are derived using.

$$F_{timer} = \frac{H_{clk}}{(Prescaler + 1) * (ARR + 1)}. \quad (8.1)$$

This allows a timer to have any frequency as a combination of these two variables. For the system, 2 different timers are used for each set of PWM outputs to allow for more customizability, and for one to be used as base time for the ADC. Since the feedback loop needs to monitor the circuit, ADCs can be used. This implementation uses one ADC that has been configured in a multichannel configuration using continuous direct memory access (DMA) instead of several ADCs available on the board. The multichannel ADC is executing its instructions synchronously with a selected timers rising edge. The ADC used is configured for single ended measurements instead of differential measurements, as we are measuring with respect to ground for any given circuit parameter, which the microcontroller is required to monitor. For the system, two timers have been used: timer 1 in the configuration PWM generation channel 1 and channel 1N and timer 3 channel 1. ADC 1 has been used with 3 single ended channels (1, 2, and 4) measuring their value relative to ground. The dead time implemented and required for safe control of the DC/AC is calculated via

$$T_{deadtime} = \frac{1}{H_{clk}} * N_{timesteps}. \quad (8.2)$$

8.4 | Voltage measurements

As the microcontroller can only measure voltages in a range from 0 to 3.3V, to measure voltages in the range of 0 to 60V additional resistances are required to protect not only the microcontroller but also to allow the microcontroller to read them accurately. Using a simple voltage divider, resistance values can be chosen to "scale" the circuit voltages down into the microcontroller range

$$V_{measured} = \frac{R1}{R2} * V_{circuit} \quad (8.3)$$

With this we chose resistance values of $R1 = 1K\Omega$ and $R2 = 20K\Omega$. Furthermore these resistances have to be high enough to pull none or little current, allowing for pure voltage sensing.

Table 8.1: Circuit voltages as measured by microcontroller

Circuit voltage	Measured voltage	Circuit Current	Measured voltage
60V	3V	10A	3.3V
50V	2.5V	8A	2.64V
40V	2V	6A	1.98V
30V	1.5V	4A	1.32V
20V	1V	2A	0.66V
10V	0.5V	1A	0.33V
0V	0V	0A	0V

As seen in Figure 8.1 this ratio allows for acceptable voltage sensing, important to consider is that the entire range of 3.3V is not used but rather stopped at 3V. This is an acceptable range, allowing still enough information for the microcontroller to read the correct voltages.

8.5 | Current measurements

As the circuit input is varying and not static, to measure the current, a separate current sensor can be used, which scales the current in the circuit. This ratio is set to 1:1000, considering the total current the circuit is able to pull before it shuts down is 10A, the current sensed by the microcontroller will be 0 to 10A which will become 0 to 10mA. This is within its maximum sink current; therefore, it can be used to

read the current. Using a resistor, this current creates a voltage drop in the range of 0 to 3.3V, which is then measured by the microcontroller via the ADC pins, allowing us to read the current of the circuit.

$$V_{measured} = I_{sensor_output} * R_{currentresistor} \quad (8.4)$$

This value was chosen as 330Ω , unlike the voltage measurements this gives the full ADC reading range, as seen in Figure 8.1. Unlike the voltage the entire range was used for the current, as this is more important when using certain types of Maximum power point transfer algorithms(MPPT), as well as to create a load detection algorithm which will have to detect fluctuations in current draw. The voltage measured by the ADC pins is then, via code related to the current we know is present in the circuit, a measurement of 3.3V on the current ADC pins relates to 10A in the circuit.

8.6 | DC/DC implementation

The DC/DC converter is a simple boost converter, which can boost input voltage by a ratio of $\frac{1}{1-D}$. Where D is the duty-cycle of the switch. The switch in this case is a MOSFET, which is driven by the PWM signals of the microcontroller, allowing us to boost voltages at different ratios depending on the algorithm, for example MPPT. In this module of the microcontroller, MPPT is also implemented. The goal of MPPT is to achieve the best possible power transfer, this is done with the ADC pins measuring voltage and current at the DC/DC input and output.

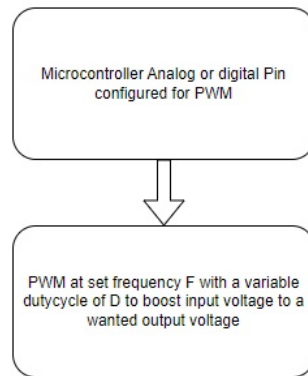


Figure 8.3: Basic DC/DC algorithm flowchart

8.7 | DC/AC implementation

The DC/AC converter used to convert our boosted DC signal to AC is controlled by 4 switches, in which there are 2 pairs of 2 MOSFETs switching complementary to each other with an inserted dead time to make sure there are no short circuits. Therefore, the microcontroller needs to output 2 complementary PWM signals with dead time to drive the MOSFETs correctly. The output signal frequency is related to the switching frequency of the switches set by the PWM of the microcontroller. In this part of the algorithm, no duty cycle changes are implemented beyond a safety algorithm if the boosted voltage is 60V or the current is 10A. For the least distortion, the signal should have a duty cycle of 0.5. Finally, load detection is done using the DC/AC, the DC/DC meaning the DC/AC will receive the inputs of the generator. If then a load is detected, the DC/DC will be turned on, and the voltage will be boosted.

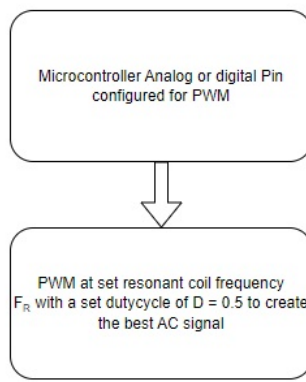


Figure 8.4: Basic DC/AC algorithm flowchart

8.8 | Maximum power point transfer

The idea behind MPPT is to increase or decrease the duty-cycle of the DC/DC converter to adjust the power conversion from the primary coil to the secondary coil. This is very important for the efficiency of the overall system, as there will always be losses in components; however, losses due to bad power conversion can be reduced significantly. There are several MPPT algorithms like: Perturbation & observation (P&O), the algorithm implemented for this converter is incremental conductance (INC). Unlike P&O, this algorithm looks not only at the power at the DC/DC converter, but the minor changes in the current, this allows a constant voltage at the MPP which cannot be done with the P&O algorithm as only powers are checked to adjust duty-cycles. A more in-depth flow chart can be found in Figure 8.5.

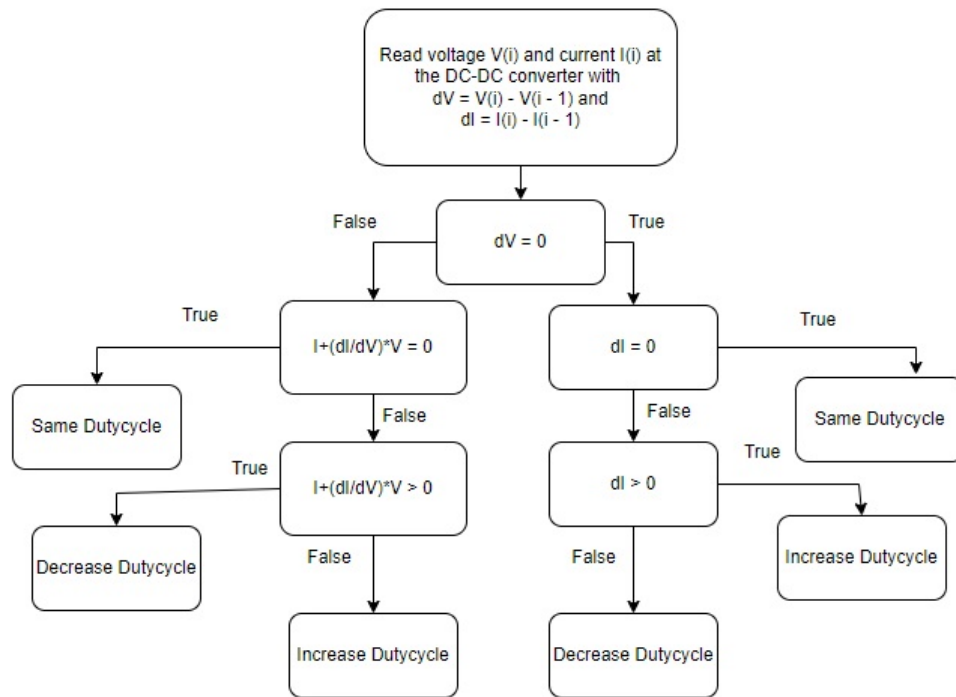


Figure 8.5: INC MPPT algorithm flowchart

8.9 | Load detection

Load detection is an algorithm in which the DC/DC converter's duty-cycle is set to 0 therefore the total input power of the system $P_{in} = V_{gen} * I_{gen}$ is also the input of the DC/AC converter. Then using current

fluctuations and changes in current draw, we can extrapolate if there is a load. Important to consider is that moving the coils around each other will induce a current, as well as the current draw will reduce depending on the distance and which the second coil is moved. If a load is detected then the DC/DC converter will be turned on and voltage will be boosted to transfer the most energy. The reason for the boost converter to start "off" is because if there is no load the boost converter will keep storing energy in the inductor and not discharge with no load to transfer the energy into. The flowchart of the algorithm can be seen in Figure 8.6.

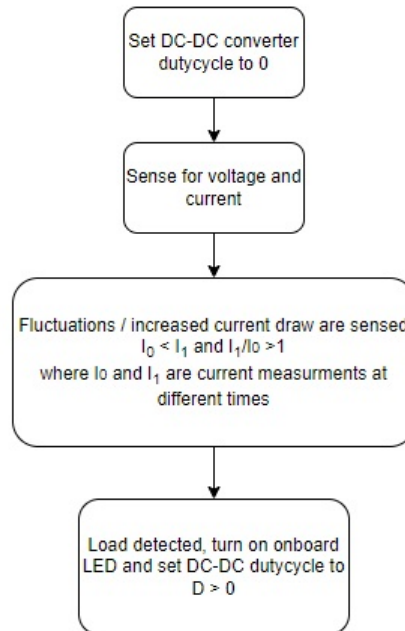


Figure 8.6: Load detection implementation

8.10 | Results

The microcontroller was a rather simple module to get to a functional state; however, it can differ a lot when looking at the creation and fine-tuning of non-essential functions such as MPPT and load detection. Furthermore, multiple microcontrollers could have been used to control the circuit; this could have been achieved through communication via USART between the microcontrollers. The final "product" that was created was one microcontroller with one tested and functional code controlling the circuit; however, the other two versions of the code (MPPT and load detection) have been implemented and functional from the code perspective but have not been tested with the circuit. This is something that can be implemented in the future to improve the efficiency and overall stability of the system. Moreover, there are several versions of load detection and MPPT algorithms that can be implemented, which might improve the system. Finally, to improve the microcontroller, optimizations can be performed on the algorithms to increase process speeds and responsiveness.

9 | Simulink model (Ivan Stojic & Youri Lamers)

9.1 | Introduction - Ivan Stojic

This project employs MATLAB Simulink to model and analyze an electrical converter system, aiming to predict real-life performance and optimize efficiency. Simulink's simulation capabilities allow for detailed examination of electrical losses and efficiency across various subsystems. Additionally, voltage and current measurements are integrated at the output of each subsystem to facilitate precise monitoring and analysis. This method enhances both the accuracy and applicability of our research, providing insights that bridge theoretical models with practical implementations. The sections below detail the subsystem configurations and the role of Simulink in refining our understanding of system dynamics.

9.2 | Analysis of the Generator Design in the Converter System - Ivan Stojic

9.2.1 | Introduction

The generator setup is a critical component in the system, responsible for converting mechanical energy into electrical energy. This section outlines the implemented design of the generator and its role in the overall system, as well as an initial concept that was considered during the project's early stages.

9.2.2 | Generator Design and Configuration

The project utilizes a Siemens GG5104 DC machine coupled to a Hubner Giessen DSG P 7.1-07-8 for efficient conversion of mechanical energy, represented by shaft speed, into electrical energy.

Configuration Details:

- **Siemens GG5104 DC Machine:** This acts primarily to translate mechanical input into electrical voltage efficiently.
- **Hubner Giessen DSG P 7.1-07-8:** Ensures that the electrical output is consistent and aligns with system requirements.
- **Measurement Instruments:** Voltmeters and ammeters monitor the output voltage and current for real-time adjustments and monitoring.

9.2.3 | Generator Acquisition

The generator component, critical for the project's energy conversion stage, has been acquired. The Simulink model for the generator is already provided, and has the specifications according to [section 3 \[5\]](#).

9.2.4 | Initial Design Concept: Simple Voltage Source and Resistor

Initially, a simpler setup was considered for the generator, consisting of only a basic voltage source and a resistor connected in series. This elementary configuration was intended to demonstrate the fundamental principles of voltage generation and resistance within an electrical circuit.

Reasons for Advancing Beyond the Initial Concept:

- **Complexity and Realism:** The initial concept, while straightforward, did not adequately represent the dynamic interactions and efficiencies required in a real-world system.
- **Scalability and Application Suitability:** It was insufficient for scaling up to meet higher power demands or for integration with more complex systems that require precise control and regulation of power output.

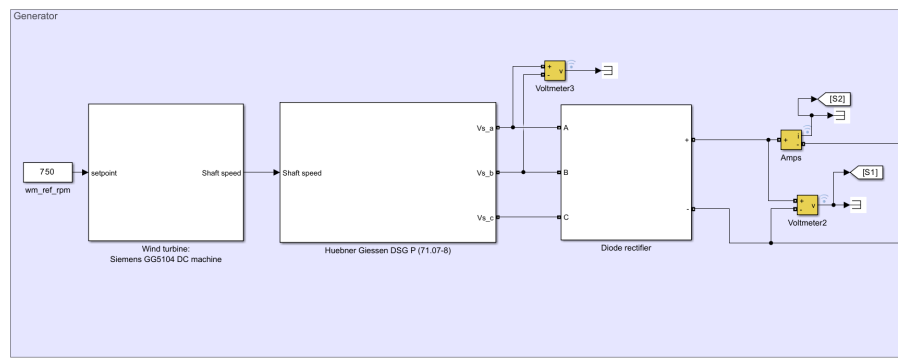


Figure 9.1: Provided simulated energy source

9.3 | Analysis of the DC/DC Converter Design - Ivan Stojic

9.3.1 | Introduction

The DC/DC converter is crucial for stabilizing and boosting the variable DC output from a generic energy source to a consistent and correct voltage level suitable for further processing or direct use. This subsection explores the chosen design of the boost converter, examining its components and their functionality within the broader context of the project. Additionally, an alternative design approach that was initially considered is discussed, focusing on its potential impacts on the system's performance.

9.3.2 | Final Design Choice: Boost Converter

Voltage Stabilization: The boost converter is utilized to manage the variable voltage levels, effectively boosting the output voltage to ensure it remains within an optimal range for efficient conversion or consumption. This capability makes the boost converter particularly versatile and suitable for a variety of applications.

9.3.3 | Component Configuration

For specific details on the components used in the boost converter, see [Table 5.5](#). The major components include:

- **Inductor (L1):** Serves as an energy storage component that smooths the flow of energy through the converter by absorbing energy during the switch's closure and releasing it when open. This action helps stabilize and boost the output against fluctuations.
- **Diode (D1):** Ensures unidirectional flow of current, crucial for maintaining the integrity and efficiency of the conversion process by preventing any reverse flow.
- **Capacitor (C1):** Stabilizes the output voltage by smoothing out any remaining fluctuations, thereby providing a steady voltage supply despite variations in input.

For a visual representation of the DC-DC Boost Converter's circuit configuration, refer to [Figure 5.1](#).

9.3.4 | Alternative Design Considerations: Enhanced Component Specifications and Configuration

Initial Concept with Enhanced Component Specifications: An alternative approach considered involved using components designed to offer better performance under varied operational conditions, aiming to enhance efficiency and reduce potential thermal and electromagnetic issues. This included:

- **High-current Inductors:** Chosen to reduce losses related to core saturation and improve efficiency under higher load conditions.
- **Fast-switching Diodes:** Selected to minimize energy losses during transitions, enhancing the overall system responsiveness and efficiency.
- **Low-ESR Capacitors:** Used to minimize voltage drops and improve the dynamic response to rapid changes in load.

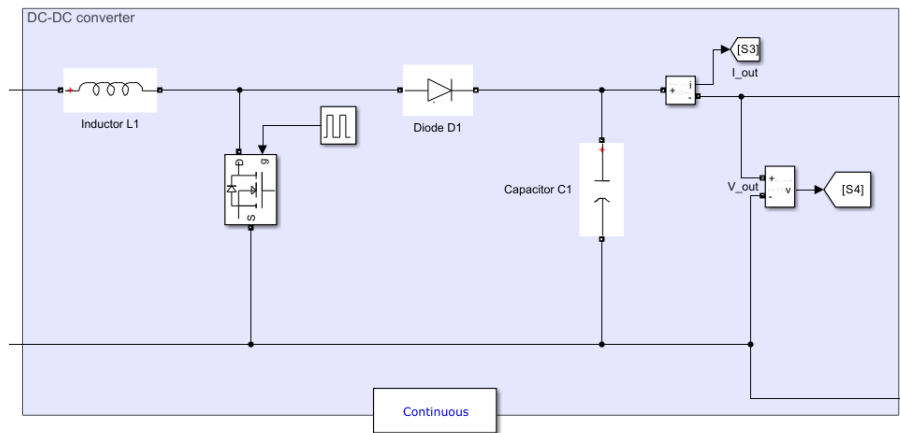


Figure 9.2: Simulated DC/DC Boost Converter.

9.4 | Analysis of the DC/AC Converter Design - Ivan Stojic

9.4.1 | Introduction

The DC/AC converter is essential for converting stabilized DC output into alternating current (AC), which is suitable for powering various loads or interfacing with the power grid. This subsection explores the design choice of the DC/AC converter, detailing the roles of its components and examining how they contribute to the project's broader goals. Additionally, an alternative design approach considered during the initial planning phase is discussed to highlight potential impacts on system performance.

9.4.2 | Final Design Choice: Full-Bridge Inverter

AC Conversion Process: The selected DC/AC converter is a full-bridge inverter, appropriate for applications requiring robust power output. This configuration efficiently converts DC power into AC power using four switches (S1, S2, S3, S4), which are controlled to alternate the DC voltage connection across the load, thus producing an AC output.

9.4.3 | Component Configuration

For specific details on the components used in the DC/AC converter, refer to [Table 5.5](#). The main components include:

- **Switches (S1, S2, S3, S4):** Typically employing MOSFETs or IGBTs, these switches handle high currents and voltages. They are controlled by a PWM (Pulse Width Modulation) signal that dictates their switching action to synthesize an AC waveform.
- **Filter (L and C):** Comprising inductors and capacitors, this filter smooths out the waveform, significantly reducing harmonic distortion in the AC output.

For a visual representation of the DC-AC Converter's circuit configuration, refer to [Figure 5.5](#).

9.4.4 | Alternative Design Considerations: Enhanced Switching Strategy and Filtering

Initial Concept with Advanced Modulation Techniques: Originally, an enhanced switching strategy was considered that employed more sophisticated modulation techniques to improve waveform quality and increase converter efficiency. This approach included:

- **Space Vector PWM:** This advanced modulation scheme was proposed to potentially reduce switching losses and achieve better utilization of the DC supply voltage.
- **Multi-level Inverter Design:** Using additional voltage levels to create a closer approximation to a sine wave, this design aimed to reduce harmonic distortion significantly without the need for extensive filtering.

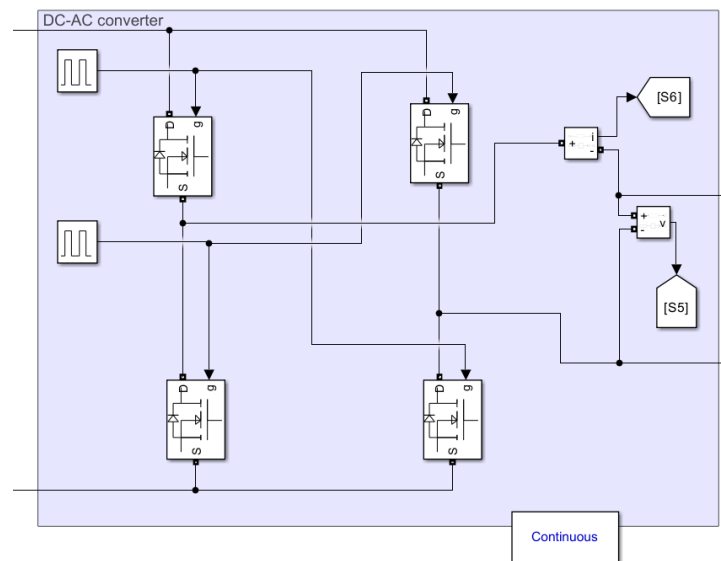


Figure 9.3: Simulated DC/AC Converter.

9.5 | Analysis of Coil Configuration in the Converter System - Ivan Stojic

9.5.1 | Introduction

The coils in the converter system are integral for energy transfer within the circuit. This section focuses on the specific coil configuration implemented and briefly touches on alternative designs considered during the initial phase.

9.5.2 | Coil Design and Configuration

The coils are arranged as coupled inductors, which are critical in ensuring efficient magnetic coupling and energy transfer between different stages of the system. This configuration is key to maintaining high performance while minimizing losses.

Key Features

- **Coupled Inductors:** The primary and secondary coils are closely coupled, a setup crucial for effective energy transfer and minimizing losses due to magnetic leakage.
- **Core Material:** The choice of core material balances magnetic permeability with core losses, which is essential for optimal performance at the operating frequencies.

For a visual representation of the Coils Configuration circuit, please refer to [Figure 6.3](#).

9.5.3 | LC Branch Configuration

The circuit diagram includes several LC branches, which are fundamental in tuning the system's response and managing energy distribution efficiently. These LC branches consist of inductors and capacitors configured to form resonant circuits, typically used to either filter or temporarily store energy in the system.

Role of LC Branches

- **Filtering:** The LC branches can act as filters to smooth out voltage or current fluctuations, thereby stabilizing the output from the coils and enhancing the overall system stability.
- **Energy Storage:** They temporarily store energy during the system's operation, which is crucial for maintaining continuous power supply during transient conditions or when there is a sudden change in load demand.

- **Resonance:** By properly tuning the values of the inductors and capacitors, these branches can also be used to set up resonance conditions, which enhance the efficiency of energy transfer within the system.

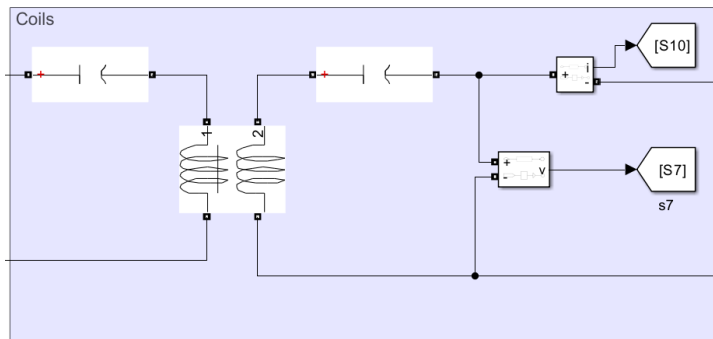


Figure 9.4: Simulated representation of Coils.

9.6 | Analysis of the AC-DC Converter Design - Ivan Stojic

9.6.1 | Introduction

The AC-DC converter is a crucial component in the system, responsible for converting alternating current (AC) from the AC output stage into a stable direct current (DC) suitable for use by various loads or for further processing. This section details the design and functionality of the AC-DC converter used in the project.

9.6.2 | Converter Design and Configuration

The AC-DC converter used in the project features a bridge rectifier arrangement composed of four diodes (D1, D2, D3, D4), which efficiently converts the incoming AC into DC. This setup is typical in many power electronic systems where reliability and simplicity are paramount.

Key Components: For specific details on the components used in the AC-DC converter, refer to [Table 5.5](#). The main components include:

- **Diodes (D1, D2, D3, D4):** These are arranged in a full-wave bridge configuration to ensure that both halves of the AC waveform contribute to the DC output. This arrangement enhances the efficiency of the conversion process.
- **Filter Capacitor (C4):** After rectification, the output contains a pulsating DC waveform, which is smoothed using a capacitor (C4). This capacitor reduces the ripple in the output voltage, providing a more stable DC supply to the load.
- **Load Resistor:** Represents the load that consumes the DC power. It is used to simulate the draw of power and to test the output stability of the converter under load conditions.

A visual representation of the AC-DC Converter's circuit configuration is shown in [Figure 5.8](#).

9.6.3 | Alternative Design Considerations: Enhanced Rectification and Filtering

Initially, advanced rectification techniques such as synchronous rectification were considered to potentially increase the efficiency of the AC-DC conversion process. These techniques employ electronically controlled switches (like MOSFETs or IGBTs) instead of diodes to reduce losses associated with forward voltage drop in standard diode rectifiers.

Benefits of Advanced Rectification:

- **Increased Efficiency:** By minimizing the voltage drop across the rectifying element, synchronous rectification can significantly enhance overall efficiency, especially useful in low-voltage applications where diode drops constitute a substantial percentage of the total voltage.
- **Improved Thermal Management:** Reduced losses translate to less heat generation, which simplifies thermal management and potentially extends the lifespan of the converter components.

Enhanced Filtering Techniques: In addition to synchronous rectification, improvements in the filtering stage were also considered. These improvements included the use of more sophisticated filter designs, such as LC filters or active filters, to further reduce ripple and improve the quality of the DC output.

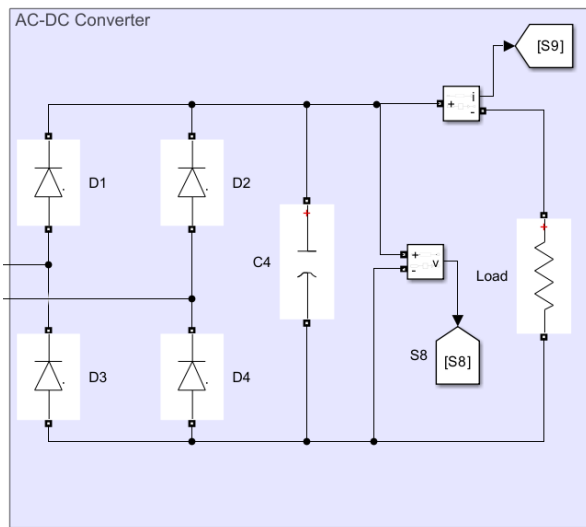


Figure 9.5: Simulated AC-DC Converter including the load.

9.7 | General Alternative Design Considerations - Youri Lamers

Not only can design alternatives be implemented in the subsystems themselves, but more general applicable design alternatives could be made to improve the accuracy of the simulation. First of all additional resistances could be placed to represent the resistance introduced by wires. Secondly, the model as of yet still lacks the modeling of thermal losses for the created subsystems which play a large part in the physical system. Additionally, more accurate component models can be implemented in the simulation to model component losses better. An example is the Simulink Simscape library which can more accurately model electrical components at the cost of it being more computationally intensive.

9.8 | Power and efficiency calculations - Youri Lamers

As mentioned before, the current and voltage at the output of each subsystem are measured making use of the Voltage Measurement and Current Measurement blocks of Simulink. These voltages V and currents I are multiplied using a product block to obtain the real-time power P at the output of each subsystem. The power is obtained using

$$P = V I. \quad (9.1)$$

Figure 9.6 shows the simulated power calculations for each subsystem.

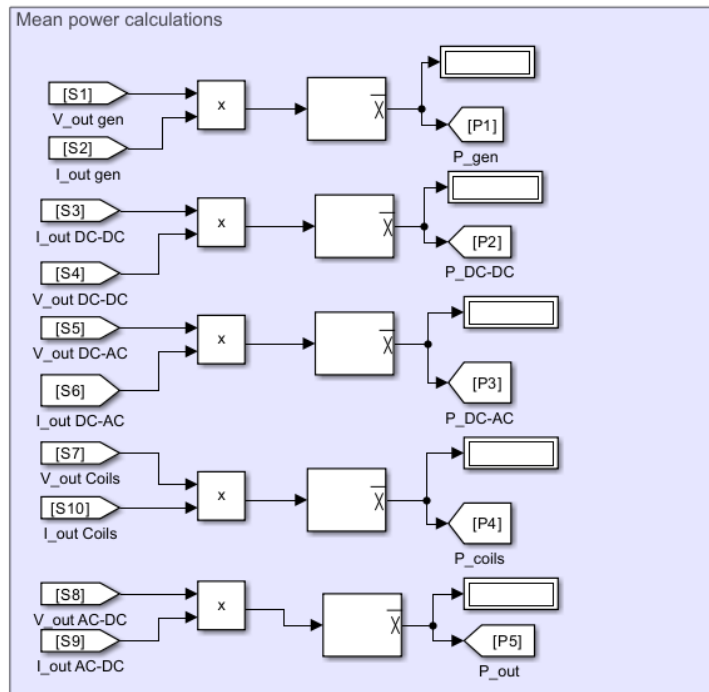


Figure 9.6: Simulated power calculations for each subsystem.

Visible in [Figure 9.6](#) is the use of mean blocks to average power results. These blocks are set to a fundamental frequency of 60Hz to minimize measurement outliers. To determine the efficiency of each subsystem, the calculated averaged output power P_o is divided by its input power P_i , which is the output power of the previous subsystem. The efficiency η is calculated using

$$\eta = \frac{P_o}{P_i} 100\%. \quad (9.2)$$

The division is done using Simulink divide blocks, while the multiplication by 100 uses gain blocks. [Figure 9.7](#) shows the simulated efficiency calculations. Visible in both [Figure 9.6](#) and [Figure 9.7](#) are the displays. The power and efficiencies shown in the displays are used for easy observations of the power and efficiency at each subsystem. However, The displays are not used for the predictions due to less accuracy than waveforms displayed in scopes.

[Table 9.1](#) shows the obtained efficiencies of each subsystem when inputting 750RPM fixed speed for the generator and a 10cm distance between the coils. It can be seen that the overall efficiency of 81.92% for the system is quite high. The most inefficient subsystem is the wireless energy transfer of the set of coils at 90.87%.

Table 9.1: Simulated efficiency for each subblock at 750 RPM fixed speed, 10cm coil distance.

Subsystem	Efficiency [%]
DC/DC Converter	97.01
DC/AC Converter	96.96
Coils	90.87
AC-DC Converter	95.84
Total efficiency	81.92

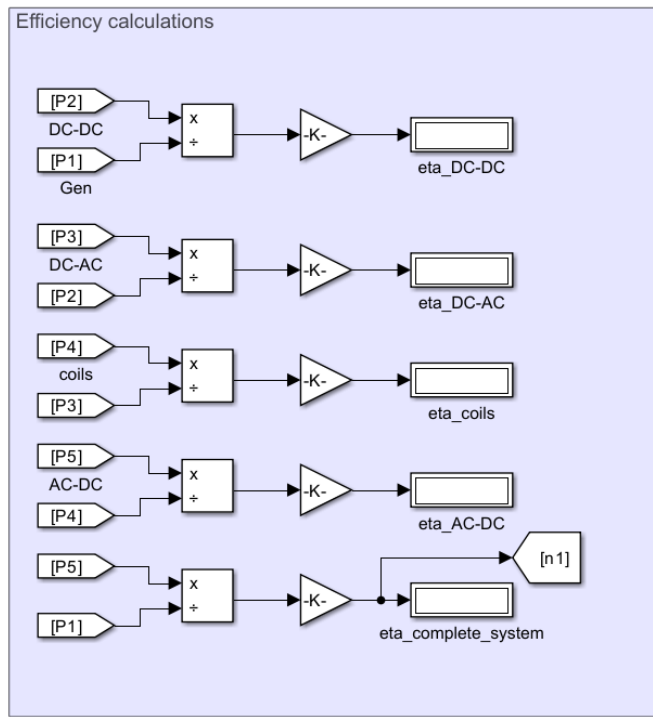


Figure 9.7: Simulated efficiency calculations for each subsystem.

9.9 | Predictions and Testing results - Youri Lamers

For the predictions, the output power and efficiency at the load are plotted in scope to show their waveforms. These waveforms are then used to obtain the average value for predicting the physical system's actual power and efficiency. The simulations are compared to measurements obtained in a demonstration session consisting of maximal 12 predefined tests. At these tests, both the input power and output power are measured and are later compared to simulation results.

Table 9.2 shows the predicted and tested results, and discrepancy for each predefined testing criterion [12].

Table 9.2: Simulated and measured testing results.

Test number	Test description	Specified [W]	Measured [W]	Error [%]
1	250 RPM fixed speed, 10cm	12.2	16.97	39.10
2	500 RPM fixed speed, 10cm	64.5	78.50	21.71
3	750 RPM fixed speed, 10cm	154	180.80	17.40
4	250 RPM fixed speed, 20cm	1.84	3.179	72.77
5	500 RPM fixed speed, 20cm	8.92	9.993	12.03
6	750 RPM fixed speed, 20cm	21.15	23.27	10.02
7	100W reached? [0 or 1]	1	1	-
8	Efficiency? [% at 100W]	80	77.36	3.3
9	Does the system find MPP? [0 or 1]	1	0	-
10	Load detection distance [cm]	25	-	-
11	Time to finish [3hrs=1, 4hrs=0.8, else=0]	-	1	-
12	PCB Design (Graded by PCB trainer)	-	5.5	-

For tests 1-3, a duty cycle $D = 0.4$ is used for the DC/DC converter during simulation, while for tests 4-6 a duty cycle $D = 0.7$ is used. Large discrepancies between 10.02% and 72.77% were obtained during testing. Noticeable is the reduction in error when the generator speed is increased. At test 3 where a measured output wattage of 180.08W is achieved, the efficiency came down to 77.36% which is only a 3.3%

error. It has to be said that during testing different duty cycle parameters were introduced compared to simulations to reduce the discrepancies. Therefore reducing the actual accuracy of the simulation. Also, it is chosen to not optimize resonant frequency for 20cm distance during tests 4-6. Therefore, both the simulated and tested output power are rather small which introduces a large error percentage at only a small absolute difference.

During testing both the systems' ability to find MPP and detect load at a certain distance were not tested due to both time constraints and problems during the measurement session. Therefore, it is decided to rather receive added points in finishing earlier, than testing MPP and load detection.

10 | Testing

10.1 | DC/DC testing (Daniel Tyukov)

Testing the DC-DC Boost Converter first tested the values on the PCB directly and, with low voltage and current, gradually increased to their operating values. The waveform we desired could be checked against the input voltage, driver signals, and gate voltage to output voltage on an oscilloscope; these problems were then debugged for issues ranging from missing connections.

When PCB testing alone did not reveal specific issues, the circuit was reassembled on a breadboard. This allowed us to determine the reasons for problems with the PCB. Afterward, the PCB was adjusted and retested. The problems identified and fixed were mentioned in 7.1.4.

To evaluate the efficiency (η) of the DC/DC converter, we used the formula:

$$\eta = \frac{V_{\text{out}} \cdot I_{\text{out}}}{V_{\text{in}} \cdot I_{\text{in}}}$$

Gradually increasing the power to 150 Watts during testing ensured a robust performance under higher loads.

10.2 | DC/AC testing (Jasper Kadijk)

Throughout the project, the inverter has been tested multiple times to fix issues and verify its performance. Firstly, tests on breadboard were carried out to verify that the design of the inverter circuit in combination with the driver circuit worked for low voltage and current. During this test, the different parts of the circuit were tested step by step. From input voltage and signal to the driver, to voltage at the gate and in the end, voltage at the output. After fixing some missing connections, a square waveform was achieved at the output. Not only did this early testing show that the design was right, it was also really useful to get acquainted with operating the oscilloscope.

After testing on breadboard, testing on the PCB could begin. This also began with testing on a load directly with low voltage and current, which were increased after. Also, the first tests with the coils utilized the DC/AC. This was a very interesting test because observations could be made on how the coils influence the behaviour of the output voltage and current. Each time testing was done, the same steps were carried out. It was important to verify the driver circuit was working as it should before turning on the power supply, to prevent components from breaking because of faulty switches or other parts.

An issue that kept on coming back when testing the whole system was a voltage drop at the auxiliary supply voltage. The team tried a lot of different things. Of course, short circuits were tested thoroughly and extra decoupling capacitors were added. Eventually, the solution was not very clear, but the problem was solved after making the whole setup neater and connecting the DC/DC converter and inverter to a different auxiliary, whereas before they were connected to the same auxiliary supply in parallel.

10.3 | Coils testing (Codrin Danculea)

The coils performance is evaluated using an impedance analyzer to measure self inductance and resistance. By connecting the oscilloscope probes to the coil terminals, voltage and current characteristics are observed to determine the induced voltage in the secondary coil when the primary coil is energized. Using the formula for mutual inductance, it can be determined using the primary current and the secondary voltage. The compensation capacitors are also measured using a multimeter to ensure that the value of the capacitors that were soldered onto a perfboard are close enough to the value that was needed to cancel out the inductance.

10.4 | Microcontroller testing (Ben Lentschig)

10.4.1 | Timers and PWM testing

The timers and PWM can be tested via an oscilloscope, measuring the PWM output pin and ground the frequency, duty-cycle and voltage swing can be measured. This has been done for the pins and configurations used (Singular PWM for DC/DC and Complementary PWM for DC/AC). Furthermore,

with the oscilloscope the dead time of the complementary PWM can be narrowed down until it reaches the best value, taking a dead time too large can affect the output signal of the DC/AC.

10.4.2 | ADC configuration testing

If the ADC or ADCs are configured, they can be tested by connecting the ADC measurement pins to either 3.3V or GND of the microcontroller, then checking if the correct values are read. After this initial test read speeds can also be adjusted.

10.4.3 | tests with circuits

Circuits need PWM outputs to drive the mosfets; therefore, tests have been conducted when circuits were created on breadboards to check if the PWM output and dead time have significant effects on losses and output signals.

10.4.4 | Planned - Entire algorithm test

After entire algorithms were created such as using ADC measurements to automatically limit duty-cycles to stay within circuit parameters such as 10A and 60V, they can be tested with the finished soldered circuit to check for any issues.

11 | Conclusions and Recommendations

11.1 | Conclusion

In conclusion, this report aims to design, build, and model a robust system that can wirelessly power a desktop PC using a sustainable energy source. A set of constraints such as a delivered minimum output power of 100W, incorporation of Maximum Power Point Tracking, and effective wireless energy transfer over a distance ranging from 10cm to 20cm are set. The system contains five key elements the energy source, the power electronic converters consisting of a DC/DC boost converter and DC/AC inverter, optimized coils, the load, and the microcontroller which regulates and enhances the wireless energy transfer. To streamline the design process, the group members are split into four subgroups covering key elements such as microcontroller, power electronic converters, PCB, and magnetics.

An overall tested peak efficiency of 77.36% is found at an output of 180.80W passing the minimum constraint of 100W. Due to time considerations and the lack of testing at beforehand, MPPT and load detection have not been implemented successfully. Furthermore, a substantial discrepancy between the MATLAB models and the physical system for both coil optimization and system representation is found. Lastly, the design of the power electronic converter topologies is successfully implemented using functioning PCB designs. All in all, the system worked feasibly but pointed out shortcomings that needed to be improved.

11.2 | Recommendation

In order to improve both efficiency, wireless energy transfer, and robustness of the system, further efforts in improving each subsystem can be made. First of all, a more efficient coil design for increased mutual inductance and a lower resistance will enhance performance further. A more detailed MATLAB optimization script could constitute a way to improve the handling of the coil parameter tuning process. From adaptive tuning to running simulations of environmental temperatures and interference effects and research into coil alignment and spacing for maximal efficiency, further research would enhance the current system and lead to research into wireless energy transfer.

Secondly, for the PCB design used for the power electronic converters, more consideration of the parasitic behavior of the circuit should have been accounted for when choosing the component placement location on the PCB. For example, by making the distance shorter between all the MOSFETs of the DC/AC, the large harmonic peaks of the output of the DC/AC circuit could have been improved.

Furthermore, further improvement on the MATLAB scripts for optimizing power losses of the component selection of the converters can be improved by more accurately representing the power losses of the different components used. Moreover, additional efforts in modeling a variable duty cycle used for MPPT could reduce the discrepancy between model and physical system.

An additional recommendation is a structure to securely mount the testing setup on to be able to present the prototype in an easier way and to accurately position the coils for maximum energy transfer.

Lastly, additional testing with load detection and MPPT on the physical prototype system could lead to the inclusion of these algorithms increasing the performance and capability of the system further.

12 | References

- [1] Exploring the potential of variable resistors, January 2024. Accessed: 2024-06-20.
- [2] Thanet Sriprom Anon Namin, Ekkachai Chaidee and Putthipong Bencha. Performance of inductive wireless power transfer between using pure sine wave and square wave inverters. *IEEE International Transportation Electrification Conference EXPO Asia-Pacific*, 2018.
- [3] B. Jayant Baliga. Inductive power transfer. *Power Electronic Handbook*, 2024.
- [4] R. Hu. *PCB Design and Layout Fundamentals for EMC*. Independently Published, 2019.
- [5] H. Huisman and G. Tibola. *Workshop 01 - Energy Source*, April 2024. 5XWF0 - CBL Wireless Energy Transfer.
- [6] Philip Machura and Quan Li. A critical review on wireless charging for electric vehicles. *Renewable and Sustainable Energy Reviews*, 104:209–234, 2019.
- [7] OpenAI. Image generated by chatgpt software, 2024.
- [8] Kavyashree Puttananjegowda, Yaoyu Cao, and Michael Greenv. Dc-dc boost converter for wireless power transfer systems. pages 0661–0665, 12 2021.
- [9] Giuseppe Schettino, Antonino Oscar Di Tommaso, Rosario Miceli, Claudio Nevoloso, Gioacchino Scaglione, and Fabio Viola. Dead-time impact on the harmonic distortion and conversion efficiency in a three-phase five-level cascaded h-bridge inverter: Mathematical formulation and experimental analysis. *IEEE Access*, 11:32399–32426, 2023.
- [10] G. Tibola. *Full Bridge Rectifier Box Specifications*, May 2024. 5XWF0 - CBL Wireless Energy Transfer.
- [11] G. Tibola. *Kick-Off Presentation*, April 2024. 5XWF0 - CBL Wireless Energy Transfer.
- [12] G. Tibola. *Study Guide*, May 2024. 5XWF0 - CBL Wireless Energy Transfer.

A | f303k8 tolerances

Table 52. Output voltage characteristics

Symbol	Parameter	Conditions	Min.	Max.	Unit
$V_{OL}^{(1)}$	Low-level output voltage for an I/O pin	CMOS port ⁽²⁾ $I_{IO} = +8 \text{ mA}$ $2.7 \text{ V} < V_{DD} < 3.6 \text{ V}$	-	0.4	V
$V_{OH}^{(3)}$	High-level output voltage for an I/O pin		$V_{DD}-0.4$	-	
$V_{OL}^{(1)}$	Low-level output voltage for an I/O pin		-	0.4	
$V_{OH}^{(3)}$	High-level output voltage for an I/O pin		2.4	-	
$V_{OL}^{(1)(4)}$	Low-level output voltage for an I/O pin		-	1.3	
$V_{OH}^{(3)(4)}$	High-level output voltage for an I/O pin		$V_{DD}-1.3$	-	
$V_{OL}^{(1)(4)}$	Low-level output voltage for an I/O pin		-	0.4	
$V_{OH}^{(3)(4)}$	High-level output voltage for an I/O pin		$V_{DD}-0.4$	-	
$V_{OLFM+}^{(1)(4)}$	Low-level output voltage for an FTf I/O pin in FM+ mode	$I_{IO} = +20 \text{ mA}$ $2.7 \text{ V} < V_{DD} < 3.6 \text{ V}$	-	0.4	

Figure A.1: F303k8 Voltage tolerances

Table 16. Voltage characteristics⁽¹⁾

Symbol	Ratings	Min.	Max.	Unit
$V_{DD}-V_{SS}$	External main supply voltage (including V_{DDA} , V_{BAT} and V_{DD})	-0.3		V
$V_{DD}-V_{DDA}$	Allowed voltage difference for $V_{DD} > V_{DDA}$	-	0.4	
$V_{IN}^{(2)}$	Input voltage on FT and FTf pins	$V_{SS}-0.3$	$V_{DD} + 4.0$	
	Input voltage on TTa	$V_{SS}-0.3$	4.0	
	Input voltage on any other pin	$V_{SS}-0.3$	4.0	
	Input voltage on Boot0 pin	0	9	
$ \Delta V_{DDx} $	Variations between different V_{DD} power pins	-	50	mV
$ V_{SSx}-V_{SSL} $	Variations between all the different ground pins ⁽³⁾	-	50	
$V_{ESD(HBM)}$	Electrostatic discharge voltage (human body model)	see Section 6.3.12: Electrical sensitivity characteristics		-

Figure A.2: F303k8 Voltage characteristics

B | Specifications IRF640NPBF MOSFET

$t_{d(on)}$	Turn-On Delay Time	—	10	—	ns
t_r	Rise Time	—	19	—	
$t_{d(off)}$	Turn-Off Delay Time	—	23	—	
t_f	Fall Time	—	5.5	—	

Figure B.1: Specifications IRF640NPBF MOSFET

C | IR2110PBF High side and low side driver circuit

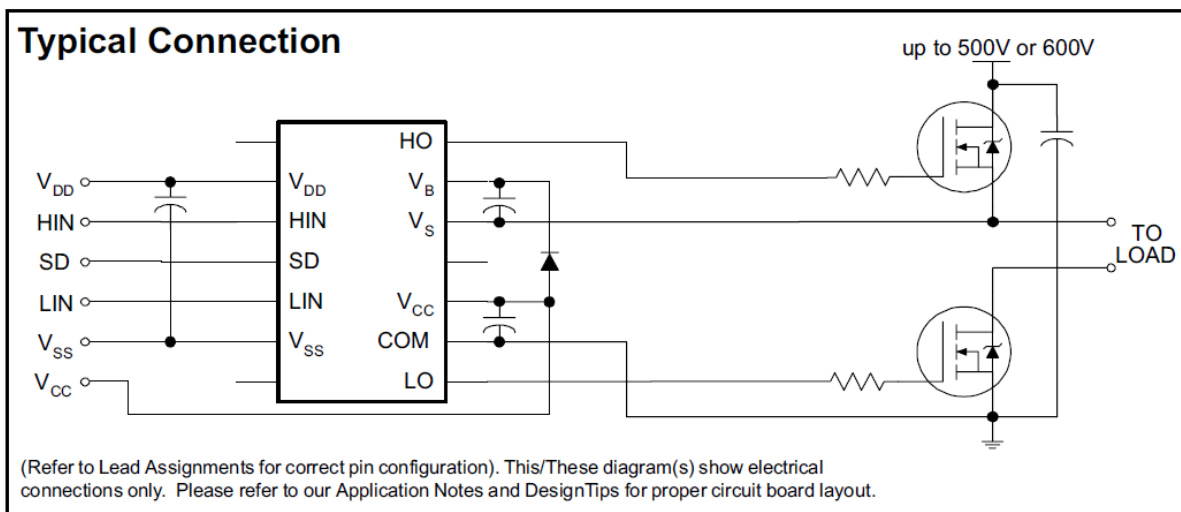


Figure C.1: High side and low side driver circuit

D | MATLAB script for DC/DC converter component selection

```

1 %% 5XWF0 Wireless energy transfer Power electronics
2
3 %% DC-DC converter
4 %% Variables
5 V_o=50; %[V] Output voltage
6 P_out = 250; %[W] Output power
7 V_in=[5,10,15,20,25,30,35,40] %[V] Input voltage.
8 I_L= P_out./V_in; %[A] Inductor Current
9
10 %% Ripples
11 delta_il= I_L %[%] Aiming for 25%
12 delta_vo= V_o.*0.05; %[%] Rule of thumb: 5%
13
14 %% Pick components ourselves
15 fs= 20000; %[Hz]
16 R=(V_o^2)/P_out; %[Ohm] Rough guess
17
18 %% Equations DC-DC
19 D= (V_o-V_in)./V_o %[-] This doesn't include the deadtime
20
21 % Inductor calculation
22 L= (V_in.*D)./(delta_il.*fs) %[H]
23 % Capacitor calculation
24 I_out = V_o./R;
25 C = (I_out.*D)./(fs.*delta_vo) %[F]
```

E | Picture of final setup

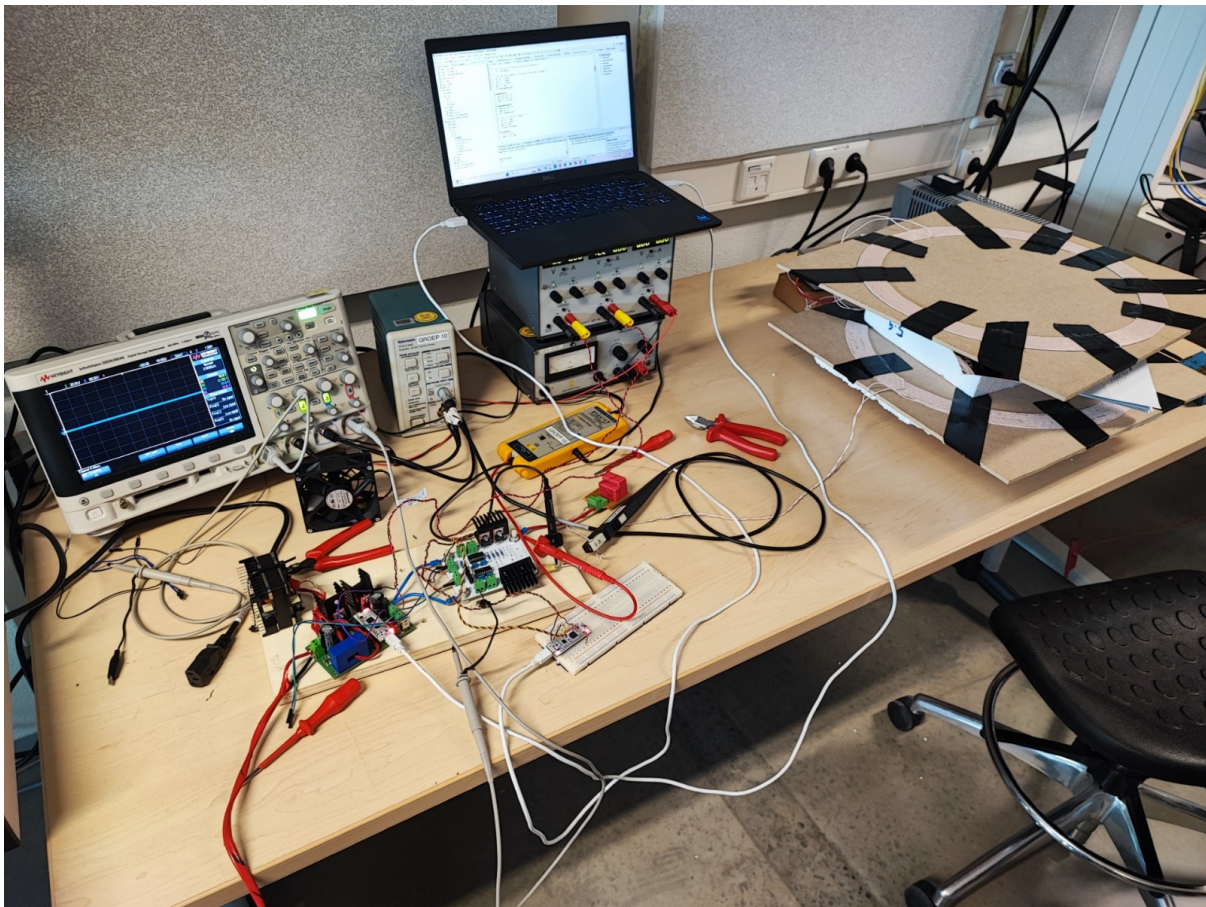


Figure E.1: Final setup before testing

F | Appendix B: Magnetics

F.1 | Optimization script

```

1 clear;
2 close all;
3
4 %% Constants
5 rho = 1.72e-8; % resistivity of copper
6 mu = 1.256629e-6; % permeability of copper
7 NumSt = 500; % number of segments for flux calculation
8 Z_load = 10; % load impedance in ohms
9 I_source = 1; % source current in amperes
10 V_in = 50; % Input voltage in volts
11 strands=140;
12 d=0.1e-3;
13
14 %% Parameter Ranges
15 n_values = 10:1:30; % Range of number of turns
16 Rp_in_values = 0.1:0.01:0.25; % Range of inner radius in meters
17 frequency_values = 40000:5000:80000; % Frequency range in Hz (excluding zero)
18
19 %% Optimization setup
20 max_efficiency = 0;
21 optimal_n = 0;
22 optimal_Rp_in = 0;
23 optimal_f = 0;
24
25 %% Main optimization loop
26 for n = n_values
27     for Rp_in = Rp_in_values
28         for f = frequency_values
29             D = 1.48e-3; % Fixed diameter of wire
30             Rp_out = Rp_in + n * D; % Calculate outer radius
31             h = 0.1; % Target distance of 10 cm
32             Rs_out = Rp_out;
33
34             if(Rp_out>0.2)
35                 continue;
36             end
37
38             r = 0;
39             flux = 0;
40             st = Rp_out/(NumSt);
41             for p = 1:n
42                 for s = 1:n
43                     [Bz, radius_secondary] = FLUXDENS(Rp_out, Rs_out, h, I_source, NumSt
44 );
45                     for j = 1:NumSt-1
46                         r = radius_secondary;
47                         flux = flux + Bz(j)* pi * (r(j + 1)^2 - r(j)^2);
48                     end
49                 end
50             end
51
52             M = flux/I_source;
53
54             % Self-inductance calculations
55             Lp = n^2 * SELF(Rp_out, Rp_in, n);
56             Ls = Lp; %change yourself
57
58             % Leakage inductance
59             a = 1; % Assuming primary and secondary have the same turns for simplicity
60             Llkp = Lp - a * M;
61             Llks = Ls - (1/a) * M;
62
63             % Resistance calculations
64             delta = sqrt(rho / (pi * f * mu)); % Skin depth
65             if delta >= (d/2) %radius of single strand
66                 ks = 1;
67             else

```

```

68         ks = delta / (d/2);
69     end
70     lturn = 2 * pi * mean([Rp_in, Rp_out]); % Average turn length
71     R_dc = (rho * 4 * lturn) / (pi * strands * d^2 * ks);
72     xs_squared = (8 * pi * f * 10^-7) / R_dc;
73     gamma_s = (xs_squared^2) / (192 + xs_squared^2);
74     R_ac = R_dc * (1 + gamma_s);
75     R_dc_tot = n * R_dc;
76     R_ac_tot = n * R_ac;
77
78     % Calculate C for target frequency
79     if Llks == 0
80         C = inf;
81     else
82         C = 1 / ((2 * pi * f)^2 * Llks);
83     end
84
85     omega = 2 * pi * f;
86
87     ZL_lkp = 1j*omega*Llkp;
88     ZL_lks = a^2*1j*omega*Llks;
89     ZC_s = a^2*1/(1j*omega*C);
90     ZC_p = 1/(1j*omega*C);
91     ZL_m = 1j*omega*M;
92     Z_load = a^2*Z_load;
93     Z_1 = (ZL_m*(ZL_lks+R_ac_tot+Z_load+ZC_s))/(ZL_m+ZL_lks+R_ac_tot+Z_load+ZC_s
94 );
95     V_1 = V_in.*.(Z_1)./(R_ac_tot+ZL_lkp+ZC_p+Z_1);
96     V_1_abs = abs(V_1);
97     I_1 = V_1./(ZL_lks+ZC_s+R_ac_tot+Z_load);
98     I_m = V_1./ZL_m;
99     I_in = V_in./(R_ac_tot+ZL_lkp+ZC_p+Z_1);
100    I_in_abs = abs(I_in);
101    V_out = I_1.*Z_load;
102    % P_out = abs(I_1).^2.*R_130.
103    P_out = (abs(V_out/sqrt(2)).*abs(I_1/sqrt(2)))
104    P_in = ((abs(V_in)/sqrt(2)).*(abs(I_in)/sqrt(2)))
105
106    efficiency = 100*P_out./P_in
107    Power = P_out
108    if abs(P_in)>=300
109        efficiency = -1
110        Power = -1
111    end
112
113    % Update max efficiency and optimal parameters
114    if efficiency > max_efficiency && P_out > 100
115        a=P_out;
116        max_efficiency = efficiency;
117        optimal_n = n;
118        optimal_Rp_in = Rp_in;
119        optimal_f = f;
120        optimal_C = C;
121        optimal_M = M;
122        optimal_L = Llks;
123    end
124 end
125 end
126
127 %% Display optimal results
128 disp(['Maximum Efficiency: ', num2str(max_efficiency)]);
129 disp(['Optimal Number of Turns: ', num2str(optimal_n)]);
130 disp(['Optimal Power ', num2str(a)]);
131 disp(['Optimal Inner Radius: ', num2str(optimal_Rp_in), ' m']);
132 disp(['Optimal Frequency: ', num2str(optimal_f), ' Hz']);
133 disp(['Capacitance: ', num2str(optimal_C), ' F']);
134 disp(['Mutual inductance: ', num2str(optimal_M), ' H']);
135 disp(['Leakage inductance: ', num2str(optimal_L), ' H']);
136 function [Bz, rs] = FLUXDENS(Rp, Rs, h, I, NumSt)
137     mu0 = 4*pi*1e-7; % Permeability of free space
138     rs = linspace(0, Rs, NumSt); % Array of radial positions where Bz is calculated
139     Bz = zeros(size(rs)); % Initialize Bz to hold the magnetic flux density results

```

```
140
141 for nn = 1:length(rs)
142     alpha = rs(nn) / Rp;
143     beta = h / Rp;
144     Q = ((1 + alpha)^2 + beta^2);
145     k = sqrt((4 * alpha) / Q);
146     [KK, EK] = ellipke(k^2);
147     B0 = (I * mu0) / (2 * Rp);
148     Bz(nn) = B0 * (1 / (pi * sqrt(Q))) * (EK * ((1 - alpha^2 - beta^2) / (Q - 4 *
149     alpha)) + KK);
150 end
```